Dark matter phenomenology of high speed galaxy cluster collisions

Yuriy Mishchenko[1] and Chueng-Ryong Ji[2]

[1] *Faculty of Engineering, Izmir University of Economics, Izmir 35330, TURKEY*
[2] *Department of Physics, North Carolina State University, Raleigh NC 27695-8202, USA*

We perform a general computational analysis of possible post-collision mass distributions in high-speed galaxy cluster collisions in the presence of weakly self-interacting dark matter. Using this analysis, we show that weakly self-scattering dark matter can impart subtle yet measurable features in the mass distributions of colliding galaxy clusters even without significant disruptions to the dark matter halos of the colliding galaxy clusters themselves. Most profound such evidences are found to reside in the tails of dark matter halos' distributions, in the space between the colliding galaxy clusters. This feature appears in our simulations as shells of scattered dark matter expanding in alignment with the outgoing original galaxy clusters, contributing significant densities to projected mass distributions at large distances from collision centers and large scattering angles up to 90°. Our simulations indicate that as much as 20% of the total collision's mass may be deposited into such structures without noticeable disruptions to the main galaxy clusters. Such structures at large scattering angles are forbidden however in purely gravitational high-speed galaxy cluster collisions. Convincing identification of such structures in real colliding galaxy clusters would be a clear indication of the self-interacting nature of dark matter. Our findings may explain the dark matter ring feature recently found in the long-range reconstructions of the mass distribution of the colliding galaxy cluster CL0024+017.

I. INTRODUCTION

Dark matter and dark energy, comprising together 95% of the energy budget in the Universe, remain among the biggest unsolved mysteries of modern physics. Dark matter (DM) has been described conventionally using the Cold Dark Matter (CDM) model, where the primary candidate for DM is an extremely massive ($m_{DM} \approx 10 - 1000$ GeV) particle interacting exclusively via the weak interaction - the so-called Weakly Interacting Massive Particle (WIMP) [1, 2]. In recent years, observations began to suggest that DM can be interacting with the cross-sections large enough to influence the formation of small-scale cosmological structures, the so called Strongly Interacting Dark Matter (SIDM) [3–12]. Recent theoretical works put forth various models of such self-interacting DM including mirror DM [13], flavor-oscillating DM [14], SIDM [15, 16], etc.

Recent observations of colliding galaxy clusters provided a unique opportunity for gaining additional insights about the properties of DM empirically [17–20]. The observed galaxy clusters may be regarded as natural astrophysical accelerators for high-energy DM particles' collisions. The observations of two or more galaxy clusters undergoing a high-speed central or near-central passage through each other after a gravitational in-fall can offer new clues about the microscopic properties of DM [17–42]. The bullet-type galaxy cluster collisions are such collisions that involve a smaller galaxy cluster, sometimes called the "bullet", falling onto a much larger cluster. In several cases of such collisions, a bullet-type galaxy cluster collision has been observed shortly after the passage of the bullet through the main cluster [21, 23]. Those observations evinced that the galaxy groups in the bullet-type galaxy cluster collisions exhibit a collisionless behavior, namely, passing through each other essentially freely without interactions. On the other hand, the gas component of such colliding galaxy clusters—the inter-cluster medium (ICM)—exhibits a drastically different behavior with significant ram friction, super-sonic bow-shocks, and strong heating accompanied by X-ray emission as witnessed [17, 18, 24, 29]. One may ask which of these components the DM halos are co-localized with. Subsequent reconstructions of the mass distribution in some of such bullet-type collisions by means of strong and weak gravitational lensing showed that the DM halos in these collisions are co-localized with the collisionless galaxy groups but not with the collisional ICM gas [17–40]. This co-localization led to conclusion that the material in the DM halos is collisionless much like the galaxy groups, rather than collisional like the ICM. Arguments such as the preservation of mass-to-light ratios and the coincidence of the centroids of DM halos with that of galaxy groups led to the constraints on the cross-section of possible SIDM particles at approximately $\sigma_{DM}/m_{DM} < 1\ cm^2 g^{-1}$ [17, 21, 22, 28, 31, 35, 43].

In this work, we perform a computational study of possible post-collision mass distributions that may be realized in high-speed collisions of galaxy clusters in the presence of weakly self-scattering DM. Several past computational studies focused on simulating the known colliding galaxy clusters and estimating the properties of the dark matter particles from that analysis [25, 28, 30, 31, 40, 44, 45]. Here, we survey rather different possibilities for post-collision mass distributions in high-speed collisions of galaxy clusters under a variety of scenarios in the presence of self-interacting DM. In that respect, our study does not focus on any specific galaxy cluster collision but aim at an explorative analysis of possible configurations that can be realized in galaxy cluster collisions in the presence of self-interacting DM. For instance, we do not specifically simulate the classical Bullet cluster 1E 0657-56 although such Bullet cluster

observations motivated our study. Our particular emphasis is to look for the effects introduced by astrophysically weak (but in terms of particles physics, potentially still quite strong) DM self-interactions in the projected mass densities of colliding galaxy clusters.

We find from our study that the DM particles interacting with $\sigma_{DM}/m_{DM} \approx 1\ cm^2 g^{-1}$ and above cause severe disruptions to DM halos of colliding galaxy clusters, leading to their rapid and complete destruction or merger, depending on the collisions' speed. Further, we find that a range of weaker DM self-interactions, $\sigma_{DM}/m_{DM} \approx 0.1\ cm^2 g^{-1}$, while not introducing major distortions to the main colliding galaxy clusters themselves, may create weak but detectable features in the mass distributions in the space outside and between the colliding galaxy clusters, that is, in the tails of their DM halos' mass distributions. One such feature is the radial shell of single-scattered DM particles formed due to the scattering of DM particles on each other during the passage of the colliding galaxy clusters through one another. These appear in the projected mass density maps as extended, spherical concentrations of DM at large distances from the collision's center and large scattering angles. Convincing observations of such features could provide clear evidence of the self-interacting nature of DM. Indeed, while these results cannot be claimed with certainty at this time, the structures resembling the above features appear in many mass reconstructions of colliding galaxy clusters in the literature [29, 35, 37, 38]. Our findings also may provide the explanation of the DM ring recently observed in the long-range mass reconstructions of the galaxy cluster CL0024+17, as the remnant of such an ancient shell of scattered DM material [27].

The remainder of the paper is organized as follows. In Section II, we discuss the methodology of our study. In Section III, we survey different types of post-collision mass distributions with respect to the parameters such as collision's speed, mass, DM self-interaction strength, etc. In Section IV, we discuss the conditions necessary for the astrophysical observation of the effects associated with the self-interacting nature of DM in galaxy cluster collisions. The summary and conclusions follow in Section V. In Appendix A, we provide the summary of the algorithms used in this work.

II. METHODOLOGY

The bulk of our study focused on carrying out a set of simulations of galaxy cluster collisions using Particle Mesh method and collisional DM particles. In this section, we discuss the details of these simulations' initialization, evaluating DM particle collisions, evaluating gravitational evolution, and selecting the simulation parameters.

A. Initial conditions

To initialize the initial positions and velocities of the particles in the DM halos of colliding galaxy clusters in the simulations below, we first prepared a "standard" equilibrated DM mass profile obtained by gravitationally relaxing DM halos in isolation for long periods of time of at least 10 Gy. First, an initial cloud of $N = 200,000$ particles was prepared with the positions and the velocities drawn randomly from $\mathcal{N}(0, R^2 \cdot I) \times \mathcal{N}(0, \sigma_V^2 \cdot I)$, where $\mathcal{N}(\mu, \Sigma)$ is the normal distribution with mean μ and covariance matrix Σ, $R = 0.25$ Mpc, and $\sigma_V^2 = -1/2\,\langle\Phi(\vec{x})\rangle$. Here, the average $\langle\Phi(\vec{x})\rangle$ is from the gravitational potential $\Phi(\vec{x})$ of the resulting mass distribution and over all the particles in the distribution, calculated in order to satisfy the Virial theorem. Each particle was assigned the mass of $1.125 \cdot 10^9 M_\odot$, for the total mass of $2.5 \cdot 10^{14} M_\odot$. Thus initialized distribution was allowed to relax in isolation for at least $T = 10$ Gy, using the Particle Mesh algorithm described below and assuming weak self-scattering of DM particles.

The mass profile obtained after the relaxation could be well described by the Plummer density $\rho(r) = \rho_0/(1 + r^2/r_0^2)^{2.5}$ [46, 47] as shown in Fig. 1. The generated profile had the total mass $M_{tot} = 2.5 \cdot 10^{14} M_\odot$, the 1/2 half-width $r_{1/2} = 0.135$ Mpc, the 1/2 projected mass profile's half-width, also known as the core radius, $r_c = 0.15$ Mpc, the Plummer density's scale parameter $r_0 = 0.24$ Mpc, and the virial radius $r_{200} = 0.6$ Mpc.

Our generated equilibrium mass profile had a soft, isothermal-like core at small distances r, different from the central cusp of the Navarro-Frenk-White (NFW) profile [48]. This was caused by DM particle collisions reducing the density of the central region and that result is consistent with the findings in the literature related to the mass profiles of SIDM halos [49–51]. Although our profile decayed as r^{-5} at large distances, much faster than r^{-3} of the NFW profile, our profile decayed rather similarly to the NFW profile (that is, close to r^{-3}) at the range of distances $(1 - 5)r_{1/2}$, that is, almost entirely out to the virial radius r_{200}, as can be seen from Fig. 1. Therefore, despite the faster drop-off rate at very large distances, our profile did provide a close approximation to the NFW mass density for the distances within the profile's virial radius, with the exception of the central cusp mentioned above.

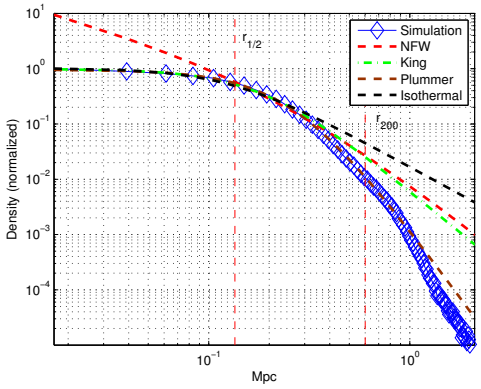

FIG. 1. The equilibrium mass profile obtained for the initial particle distributions in our simulations, blue diamonds. Red dashed line is the best tail-fit using the NFW profile $\rho(r) = \rho_0/(r/r_c)(1+r/r_c)^2$ [48], green dash-dot line is the fit using the approximate King profile $\rho(r) = \rho_0/(1+r^2/r_c^2)^{3/2}$ [21, 28], black dashed line is the fit using the isothermal profile $\rho(r) = \rho_0/(1+r^2/r_c^2)$ [47] and brown dashed line is the fit using the Plummer density $\rho(r) = \rho_0/(1+r^2/r_0^2)^{5/2}$ [47]. The profile's 1/2 half-width, $r_{1/2}$, and the virial radius, r_{200}, are also shown for reference.

B. Simulation of DM particle-particle interactions

In order to model non-gravitational interactions (that is, DM particle-particle scatterings) during the simulations of galaxy cluster collisions with self-interacting DM, we adopted the principle that two simulation particles could scatter on each other if and only if they occupied the same cell of the simulation's spatial grid $\mathcal{G}$ (the definition of $\mathcal{G}$ will be given in the next section, Section II C). For each pair of such particles, then, a scattering was enacted with the probability

$$P = \alpha V_{rel} \Delta t, \tag{1}$$

where $V_{rel} = |\vec{v}_1 - \vec{v}_2|$ is the relative speed of the two particles, Δt is the simulation's time step, and α is an effective numerical parameter used to control the strength of the DM self-scattering in the simulations. This parameter can be related to the more commonly used ratio of the DM particles' cross-section and mass as

$$\frac{\sigma_{DM}}{m_{DM}} = \alpha \frac{N_{tot} d^3}{M_{tot}}, \tag{2}$$

where M_{tot} is the total mass of the simulated system, N_{tot} is the total number of particles in the simulation, and d is the resolution of the simulation's grid $\mathcal{G}$ (see Section II C).

The scatterings for selected pairs of particles were evaluated as follows. First, the Center-of-Mass velocity, $\vec{V}_{CM} = (\vec{v}_1 + \vec{v}_2)/2$, and the relative speed, $V_{rel} = |\vec{v}_1 - \vec{v}_2|$, of the pair were computed. Then, a new direction for the relative velocities, $\vec{n}$, was selected uniformly at random on unit sphere, assuming that the modeled DM particle-particle collisions were elastic and isotropic. In particular, for elastic and isotropic collisions of identical elementary particles the magnitude of the relative velocities needs to be preserved in the collisions while the direction of the relative velocities may change arbitrarily. Accordingly, the velocities of the particles after the scattering event can be updated as follows,

$$\begin{aligned} \vec{v}_1' &= \vec{V}_{CM} + V_{rel}\vec{n}, \\ \vec{v}_2' &= \vec{V}_{CM} - V_{rel}\vec{n}. \end{aligned} \tag{3}$$

The details of the DM particle-particle scattering algorithm are presented as Algorithm 1 in Appendix A.

C. Simulation of the gravitational evolution of DM halos

For the simulations of the galaxy cluster collisions in the presence of weakly self-scattering DM, we implemented in Matlab the Particle Mesh algorithm for N-body gravitational dynamics. In the Particle Mesh algorithm, the

gravitational evolution of a continuous spatial distribution of mass $\rho(\vec{x},t)$ is modeled by using a collection of N particles $\vec{r}_i(t)$, $i = 1 \dots N$, distributed according to $\rho(\vec{x},t)$. As the particles move in the common gravitational potential $\Phi(\vec{x},t)$, we numerically calculate $\Phi(\vec{x},t)$ by approximating $\rho(\vec{x},t)$ on a 3 dimensional grid $\mathcal{G}$ by counting the number of the particles in each grid cell, $n(\vec{x}_{\mathcal{G}},t)$, and then solving the Poisson equation,

$$\nabla^2\Phi(\vec{x},t) = 4\pi G n(\vec{x},t), \tag{4}$$

where G is the gravitational constant. A particularly advantageous method for obtaining the numerical solutions of Eq. (4) on $\mathcal{G}$ is to use the Fourier transform, $\tilde{\Phi}(\vec{k},t) = \int d\vec{x}(2\pi)^{-3/2}e^{-i\vec{k}\cdot\vec{x}}\Phi(\vec{x},t)$, whereas Eq. (4) becomes equivalent to an algebraic equation,

$$\tilde{\Phi}(\vec{k},t) = -4\pi G\frac{\tilde{n}(\vec{k},t)}{\vec{k}^2}. \tag{5}$$

Therefore, $\Phi(\vec{x},t)$ can be computed by performing two discrete fast Fourier transforms, $n(\vec{x},t) \to \tilde{n}(\vec{k},t)$ and $\tilde{\Phi}(\vec{k},t) \to \Phi(\vec{x},t)$, and making use of Eq. (5) in between. Once $\Phi(\vec{x},t)$ had been computed, the speed and the positions of all the particles in the common gravitational potential are updated according to the usual Newtonian dynamics. An additional step is performed after the step for the simulation of the DM particle-particle scatterings as described in Section II B. The simulation is then advanced in time using an adaptive time step Δt, which is set by restricting the maximum change in the speed and the position of the simulation particles and typically varies between 0.1 My and 10 My.

Our Particle Mesh algorithm is presented as Algorithm 2 in Appendix A. The algorithm requires several input parameters specifying the total real mass of the simulated collision, M_{tot}, the number of simulated particles in the first and second colliding galaxy clusters, $N1$ and $N2$, the kinetic parameter, $\Delta V2$, controlling the collision's velocity as the square of the galaxy clusters' in-fall speed at infinity, the initial offsets of the colliding galaxy clusters, $\Delta R1$ and $\Delta R2$, and the impact parameter Δb. The other algorithm's parameters include the number of cells D to be used along each dimension in the cubic spatial grid $\mathcal{G}$, with the total D^3 cells, and the cells' real size d. The total linear size of the region of space covered by the simulation is Dd.

The algorithm consists of several modules. First, the particle distributions in the DM halos of the two colliding galaxy clusters were initialized. For that, $N1$ and $N2$ particles were randomly drawn from the standard equilibrium mass profile prepared in Section II A and put into the particle clouds of the first and second galaxy clusters, respectively. Each draw implied choosing together the position and the velocity of one of the particles from the "standard" initial distribution, as defined relative to the galaxy cluster's center. Each particle was assumed to carry the same mass, $M_{tot}/(N1 + N2)$, and thus the ratio $N1/N2$ defined the ratio of the total mass in the first and second DM halos, respectively.

The equilibrium mass profile discussed in Section II A has a standard mass of $M_{std} = 2.5 \cdot 10^{14} M_{\odot}$. Most of our simulations were performed with this total mass. If simulated halos had a different mass, M'_{halo}, such as in the simulations of asymmetric galaxy cluster collisions, the positions and the velocities of the particles were additionally rescaled by the factor $(M'_{halo}/M_{std})^{1/3}$. As discussed in Section II D, the total mass in a gravitational simulation can be excluded from the equations of motion by rescaling the distances $(M_{tot}/M_{std})^{1/3}\vec{r} \to \vec{r}$, where M_{std} is a certain standard mass scale. Therefore, the equilibrium mass profiles for the total mass different from that in Section II A can be obtained by rescaling the positions and velocities of the particles as described above.

Once the particle clouds corresponding to the DM halos of the first and second colliding galaxy clusters were prepared, they were translated along the collision axis, here chosen as the x-axis, to their initial displacements $-\Delta R1$ and $\Delta R2$. In addition, one of the halos was translated along the axis perpendicular to the collision axis, here chosen as the y-axis, by the amount equal to the impact parameter Δb. Finally, for the given two particle clouds, the net overall velocities towards each other along the x-axis were computed using $\sqrt{2E_G/M_{tot} + \Delta V2}$, where E_G was the mutual gravitational energy of the two galaxy clusters at the relative separation $\Delta R1 + \Delta R2$ and $\Delta V2$ was the aforementioned parameter controlling the overall speed of the collision.

After the initial particle distributions of either DM halo were prepared, the particles were evolved using the Particle Mesh algorithm as described above for a predetermined duration of time. The time step Δt in the evolution was chosen from the condition that the largest change in the position of a particle in the simulation, $\vec{v}_i\Delta t$, remained below a certain threshold, set as the cell half-size $d/2$, and the largest gravitational change in the speed of a particle, $\vec{a}_i\Delta t$, where $\vec{a}_i$ is the i^{th} particle's gravitational acceleration, remained below a fixed threshold Δv_{max}.

D. Simulation parameters

We performed our simulations on the super-computing infrastructure of the National Energy Research Scientific Computing Center (NERSC). For the majority of our simulations, we used $N = 2 \cdot 10^5$ particles, a grid of $D^3 = 400^3$

cells, and the resolution $d = 15$ kpc, covering a cubic region of space of 6 Mpc on the side. We only simulated the dynamics of the DM halos and ignored the ICM or the visible galaxies' contribution. All simulations were performed for a fixed duration of time t_{max} of 1.5 Gy to 3 Gy, chosen to span a single passage of the colliding DM halos through each other with the adaptive time step Δt of at most 10 My.

Our survey involved the simulations of various scenarios for galaxy cluster collisions with respect to the collision's speed (or equivalently, the initial in-fall velocity of the colliding galaxy clusters $\Delta V2$), the centrality (quantified by the impact parameter Δb), the similarity of the colliding galaxy clusters' sizes (quantified by $N1/N2$), and the DM self-interaction strength as expressed by the effective strength parameter α (or equivalently, σ_{DM}/m_{DM} given by Eq. (2)).

The simulations were initialized with the two DM halos of total mass $M_{tot} = 2 \times 2.5 \cdot 10^{14} M_{\odot}$ divided into two colliding clusters, placed at the separation of $\Delta R = 2Mpc$ initially and moving towards each other with the velocities ranging from 500 kmps to 4400 kmps. In the case of the simulations of symmetric galaxy cluster collisions, the two DM halos were initialized each having the mass of $M_{halo} = 2.5 \cdot 10^{14} M_{\odot}$. In the case of asymmetric collisions, the same total mass was divided between the galaxy clusters in the ratio 5:1. This choice was made following the mass split in the Bullet cluster [19, 23, 32]. In the case of the simulations of off-central collisions, the center of the smaller halo was shifted with respect to the larger halo in the direction perpendicular to the collision axis by the amount of the impact parameter Δb equal to the core radius of the larger of the colliding clusters. This value of Δb was chosen to maximize the effect on the non-centrality in the post-collision mass distributions, whereas the larger values of the impact parameter were taken to result in the halos essentially missing each other's dense cores and the smaller impact parameters were taken to result in post-collision mass distributions not much different from fully central collisions.

In our simulations, the total mass of the collisions was not varied. This choice was made because the total mass can be reduced from gravitational equations of motion, $\frac{d\vec{v}(\vec{r},t)}{dt} = -G\nabla \int d^3r' \frac{\rho(\vec{r}',t)}{|\vec{r}-\vec{r}'|}$, by suitably re-scaling the distances such as $(M_{tot}/M_{std})^{1/3}\vec{r} \to \vec{r}$, where M_{std} is a certain standard mass scale. Therefore, the simulations of the collisions of galaxy clusters with a different total mass could be reduced to the simulation of a similar collision with a standard mass by rescaling the distances. In our simulations, the total collision mass M_{tot} was held constant at $5 \cdot 10^{14} M_{\odot}$, as mentioned above.

The full list of the parameters used for each class of our simulations is given in Table I.

III. RESULTS

A. Phenomenological characterization of different galaxy cluster collisions

The study in this works is concerned with characterizing the effects of astrophysically weak DM particle-particle self-interactions on projected mass distributions in collisions of galaxy clusters. By "weak", it is meant that DM self-interactions result in the fractions of DM particles scattered in collisions significantly less than one, namely in the order of $0.1 - 0.2$ or less. From the very nature of such weak effects, it is clear that such effects would appear, if at all, in the tails of the DM mass distributions of colliding galaxy clusters. To make such effects discernible, one needs to choose a suitable way to visualize the tails of DM mass distributions graphically. One advantageous approach for such a visualization is to use the logarithmic scale for plotting the projected mass density maps. This is the approach adopted in this paper for all illustrations and plots found below.

In our simulations, we notice that the general profile of the post-collision mass distributions of colliding galaxy clusters can be very well characterized in terms of just main three phenomenological parameters — the collision's kinetic parameter $k = |E_K/E_G|$ as defined by the ratio of the relative kinetic energy of the colliding galaxy clusters and their mutual gravitational energy, the fraction a of DM halos' mass scattered non-gravitationally, and the post-collision separation of the outgoing galaxy clusters in terms of their typical radius ratio r/r_c.

The notion of the kinetic parameter $k = |E_K/E_G|$ is advantageous for characterizing the degree impact produced by gravitational effects in the post-collision mass distribution. Intuitively, for small values of k the colliding galaxy clusters are slow and one can expect that gravitational interactions will play an important role in the post-collision mass distribution. For large values of k, however, one understands that the colliding galaxy clusters will essentially fly through each other experiencing little gravitational interaction.

In our definition $k = |E_K/E_G|$, the value of k depends on where exactly the kinetic and gravitational energies are measured during the collision. To be specific, we define k as the ratio of the kinetic energy to the mutual gravitational energy of the colliding galaxy clusters at the point of closest approach. Thus, we have $k = 1$ for an in-fall from zero-velocity at infinity and $k > 1$ implies a collision with a non-zero initial in-fall velocity, while $k < 1$ implies slower collisions such as resulting from the galaxy clusters in-falling from a smaller distance, having completed initial passage through each other or having collided with another galaxy cluster nearby.

TABLE I. The parameters of the simulations of different galaxy cluster collision scenarios performed in this work.

Type of scenario	M_{tot} ($M_\odot$)	D (#)	Dd (Mpc)	$N1$ (10^5)	$N2$ (10^5)	$\Delta V2$ (kmps^2)	$\Delta R1$ (Mpc)	$\Delta R2$ (Mpc)	Δb (Mpc)	$\frac{\sigma_{DM}}{m_{DM}}$ ($cm^{-2}g$)	k	a (%)
fast CDM	$5 \cdot 10^{14}$	400	6.0	1.0	1.0	1300^2	1.0	1.0	0.0	0.0	1.6	-
free-fall CDM	$5 \cdot 10^{14}$	400	6.0	1.0	1.0	0.0	1.0	1.0	0.0	0.0	1.0	-
slow CDM	$5 \cdot 10^{14}$	400	6.0	1.0	1.0	$-(700^2)$	1.0	1.0	0.0	0.0	0.8	-
symmetric-central-weak	$5 \cdot 10^{14}$	400	6.0	1.0	1.0	1300^2	1.0	1.0	0.0	0.45	1.6	10
symmetric-central-strong	$5 \cdot 10^{14}$	400	6.0	1.0	1.0	1300^2	1.0	1.0	0.0	1.80	1.6	40
symmetric-noncentral-CDM	$5 \cdot 10^{14}$	400	6.0	1.0	1.0	1300^2	1.0	1.0	0.25	0.0	1.6	-
symmetric-noncentral-weak	$5 \cdot 10^{14}$	400	6.0	1.0	1.0	1300^2	1.0	1.0	0.25	0.45	1.6	7
symmetric-noncentral-strong	$5 \cdot 10^{14}$	400	6.0	1.0	1.0	1300^2	1.0	1.0	0.25	1.80	1.6	31
asymmetric-central-CDM	$5 \cdot 10^{14}$	400	6.0	1.5	0.3	800^2	0.0	2.0	0.0	0.0	1.4	-
asymmetric-central-weak	$5 \cdot 10^{14}$	400	6.0	1.5	0.3	800^2	0.0	2.0	0.0	0.50	1.4	7
asymmetric-central-strong	$5 \cdot 10^{14}$	400	6.0	1.5	0.3	800^2	0.0	2.0	0.0	3.25	1.4	60
asymmetric-noncentral-CDM	$5 \cdot 10^{14}$	400	6.0	1.5	0.3	800^2	0.0	2.0	0.25	0.0	1.4	-
asymmetric-noncentral-weak	$5 \cdot 10^{14}$	400	6.0	1.5	0.3	800^2	0.0	2.0	0.25	0.80	1.4	9
asymmetric-noncentral-strong	$5 \cdot 10^{14}$	400	6.0	1.5	0.3	800^2	0.0	2.0	0.25	4.05	1.4	58
very fast collisions comparison	10^{15}	100	6.0	1.0	1.0	5400^2	1.0	1.0	0.0	0.45	8.0	7
very fast collisions comparison	10^{15}	100	6.0	1.0	1.0	3500^2	1.0	1.0	0.0	0.45	4.0	8
very fast collisions comparison	10^{15}	100	6.0	1.0	1.0	2000^2	1.0	1.0	0.0	0.45	2.0	10
very fast collisions comparison	10^{15}	100	6.0	1.0	1.0	1400^2	1.0	1.0	0.0	0.45	1.5	11

The fraction of the DM halos' mass scattered in a collision via DM particle-particle scattering, a, is another important phenomenological parameter for galaxy cluster collisions. It is the only "physical" observable related to DM self-interactions, which can be measured from the simulations directly. This ratio serves as the bridge for connecting the simulation's DM self-interaction strength parameter α with the physically interesting quantity such as σ_{DM}/m_{DM}.

The fraction a quantifies phenomenologically the degree of impact that DM self-interactions have on the post-collision mass distribution of a galaxy cluster collision, by setting the upper limit on the relative weight of the features contributed by DM particle-particle interactions to such distribution. For instance, if in a collision of galaxy clusters $a = 0.1$, that is, 10% of DM halos' mass undergo nongravitational scattering, then it is immediately clear that the DM self-interaction features can comprise at most 10% of the post-collision mass distribution.

The fraction a is related to the effective DM self-interaction parameter α and the physical DM self-interaction parameter such as σ_{DM}/m_{DM}. While it can be calculated theoretically from σ_{DM}/m_{DM} given the knowledge of the mass distribution in the colliding galaxy clusters, it can be also estimated straightforwardly from the simulations. Thus, the two quantities can be related to each other. The fraction a also can be estimated astrophysically under certain conditions as discussed below, which is an important advantage of this quantity.

For concreteness, we set

$$a = 2N_{12}/(N_1 + N_2) = (\delta M_1 + \delta M_2)/M_{tot}, \tag{6}$$

where N_{12} is the number of simulated DM particle-particle scattering events between the particles from the two colliding halos, and $N_1 + N_2$ is the total number of the particles in the simulation, whereas $\delta M_{1,2}$ are the real masses of the first and second colliding DM halos being scattered via DM particle-particle collisions and M_{tot} is the combined mass of that halos.

The post-collision separation of colliding galaxy clusters is another advantageous descriptor for characterizing specifically the stage of a galaxy cluster collision. In general, we observe in our simulations that the post-collision mass distribution in different collisions share significant similarities for the same separations of the galaxy clusters, expressed in the terms of a typical distance scale associated with the colliding galaxy clusters' size. Such separation is therefore advantageous for characterizing the stage of the post-collision evolution of the colliding galaxy clusters in place of regular time. Another advantage of that quantity is that it can be related directly to astrophysical data. For concreteness, we define such separation as the ratio of the distance r between the centers of the outgoing galaxy clusters and the core radius r_c of the larger of the galaxy clusters, defined as the 1/2 half-width of the projected mass distribution of that galaxy cluster's DM halo.

B. The phenomenology of high-speed galaxy cluster collisions in CDM model

We first review our simulations of high-speed collisions of galaxy clusters in standard CDM, that is, when the gravity is the only force affecting the colliding galaxy clusters. Specifically, we turn our attention to the central collisions of two equal-size galaxy clusters. In such a case, the collision contains only two free parameters, M_{tot} and $k = |E_K/E_G|$, of which the total mass can be excluded by rescaling the distances as discussed above, leaving only a single parameter k that completely characterizes such galaxy cluster collision in CDM.

As discussed in Section III A, the kinetic parameter k defines the relative importance of kinetic versus gravitational effects in the collision. By the conservation of energy, k is related to the total energy of the colliding galaxy clusters, E, and their mutual gravitational energy, E_G, as $k = 1 + E/|E_G|$. Thus, three essentially different regimes can be distinguished: fast collisions with $E > 0$ and $k > 1$, "free-fall" collisions with $E = 0$ and $k = 1$, and slow collisions with $E < 0$ and $k < 1$. In fast collisions, the clusters fall towards each other from a finite in-fall velocity at infinity. In "free-fall" collisions, the clusters fall towards each other from zero speed at infinity. The case $k < 1$ corresponds to the situation where the clusters fall towards each other from zero speed at the smaller distance.

For fast collisions, $k > 1$, our simulations indicate two additional regimes of very fast collisions, $k > 2$, and fast collisions, $2 > k > 1$. For very fast collision, $k \approx 2$ and above, the colliding galaxy clusters pass through each other without significant gravitational distortions, essentially maintaining their shape and velocity after the collision.

For fast collisions, $2 > k > 1$, the galaxy clusters are observed to substantially interact gravitationally during the collision, forming extensive high-velocity ejecta in the form of forward conic jets surrounding the clusters' initial velocity vectors. These ejecta give the projected mass densities, when plotted on a log-scale, a notable forward "triangular" or "fan-out" shape, as shown in the left panel of Fig. 2. A narrow and weak "central bridge" of slow material trailing in-between and behind the outgoing galaxy clusters also can be observed in this regime under certain conditions.

An important observation, however, is that the ejecta in these regimes are always formed in forward and backward cones around the collision axis, restricted to small scattering angles. This is consistent with the general properties of the differential cross-section of gravitational interaction, which has large cross-section for small scattering angles and dramatically smaller cross-section towards 90° and even smaller cross-sections at 180° scattering angle.

For "free-fall" case, $k = 1$, we observe that the colliding galaxy clusters merge or nearly-merge typically after a single passage. The merger produces a profound amount of ejecta surrounding the merging galaxy clusters. It appears in the log-scale projected density maps as a characteristic "butterfly" shape as shown in the central panel of Fig. 2.

In slow collisions, $k < 1$, the clusters are always seen to merge rapidly, generating a large amount of ejecta in all directions, as shown in the right panel of Fig. 2.

We once again note that Fig.2 as well as all other figures in this paper show the simulated projected mass density maps on logarithmic scale, with the contour-lines showing the density levels of such maps normalized to the peak projected mass density of one.

C. The phenomenology of high-speed galaxy cluster collisions in interacting DM models

In the interacting DM case, the phenomenology of high-speed galaxy cluster collisions is governed primarily by two parameters: the kinetic parameter k and the effective DM scattering parameter a. The kinetic parameter k was defined above as the ratio of the colliding galaxy clusters' kinetic energy to their mutual gravitational energy taken

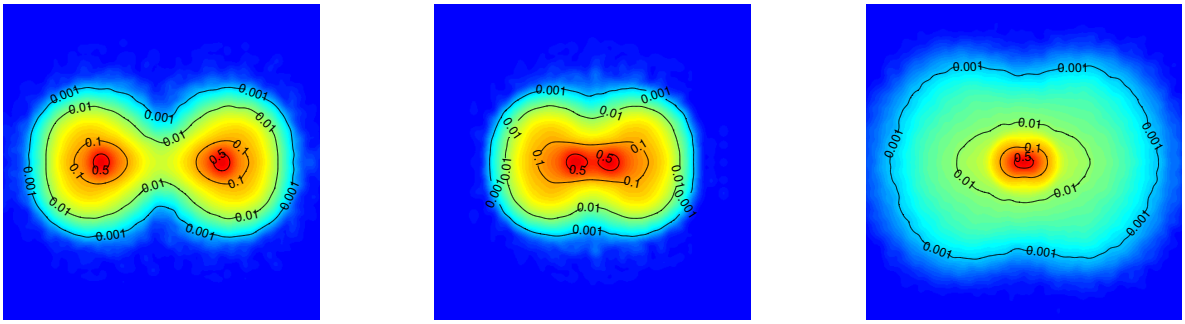

FIG. 2. Possible phenomenologies of the projected mass density profiles of galaxy cluster collisions in CDM model, for different values of the kinetic parameter k. From left to right shown are the examples of a central symmetric fast collision ($k = 1.6$, separation $15r_c$), a "free-fall" collision ($k = 1.0$, maximum separation of approximately $6r_c$), and a slow collision ($k = 0.8$, final merger configuration). The simulation parameters are as defined in Table I. The projected mass density maps are shown color-coded according to logarithmic scale, with the contour-lines showing the density levels of such maps normalized to the peak projected mass density of one.

at the point of closest approach. The effective DM scattering strength a is defined as the fraction of DM halos' mass scattered during the collision via non-gravitational DM self-interactions.

The choice and nature of these parameters were discussed in Section III A in some detail. Here, we only add that the DM scattering fraction a can be often approximately calculated using the formula frequently used in the literature, $a \approx \frac{\sigma_{DM}}{m_{DM}}\Sigma_M$, where Σ_M is the average projected mass density of the smaller of the colliding galaxy clusters calculated over some area. This formula can be taken as an approximate order of magnitude relationship between a and σ_{DM}/m_{DM}. For more accurate relationship, the calculation should take into account the mass profiles of the colliding galaxy clusters, their speeds, and the impact parameter.

In the phenomenology of galaxy cluster collisions with self-interacting DM, we encounter three main situations with respect to the value of the kinetic parameter k as discussed before, namely, fast, "free-fall", and slow collisions. In the cases of slow and free-fall collisions, we find that the large amount of gravitational ejecta drastically obscures the effects of weak DM self-scattering. Thus, we focus further on the fast and very fast collision scenarios, $2 > k > 1$ and $k > 2$, respectively.

With respect to the DM self-scattering strength, we observe three main regimes depending on the value of the parameter a, namely, strong scattering $0.5 \leq a$, weak scattering $a \leq 0.2$, and intermediate scattering $0.2 \leq a \leq 0.5$. In our simulations, these correspond roughly to $\sigma_{DM}/m_{DM} > 2\ cm^{-2}g$ for strong, $\sigma_{DM}/m_{DM} < 0.5\ cm^{-2}g$ for weak, and $0.5\ cm^{-2}g < \sigma_{DM}/m_{DM} < 2\ cm^{-2}g$ for intermediate scattering regime (see Table I). The typical forms of the post-collision mass distribution in these regimes are shown in Fig. 3, as a table with the columns corresponding to different DM self-interaction strengths and the rows corresponding to different collision scenarios such as symmetric central, asymmetric central, symmetric non-central and asymmetric non-central.

In all regimes, we observe that the DM self-interactions result in additional component introduced into the projected mass density maps and appearing as a diffuse circular mass concentration centered at the collision's center and extending radially in all directions out to the distances comparable with that of the outgoing galaxy clusters from the collision center. The most significant difference in these density maps is the presence of DM ejecta observed at large, close to 90° scattering angles, that is, perpendicular to the axis of the collision. As we have discussed in the previous section, purely gravitational effects cannot produce such ejecta. Therefore, observations of DM concentrations at equatorial planes of galaxy cluster collisions could provide a strong evidence of the self-interacting nature of DM.

The relative weight of such additional DM density component increases with the strength of DM self-interactions. In particular, in the case of strong DM particle-particle scattering, $a \approx 0.5$ and above or $\sigma_{DM}/m_{DM} \approx 2\ cm^{-2}g$ and above, we observe that the mass distribution of the colliding galaxy clusters is disrupted significantly in all scenarios, as shown in the third column of Fig. 3. In many cases, a very wide single approximately spherical hot cloud of DM material forms around the collision's center as shown in the first and third rows of Fig. 3. In the case of asymmetric bullet-type collisions, the halo of the "bullet" cluster typically does not survive the passage through the main cluster, whereas such minor halo is nearly completely dispersed after the passage and only appears in the projected mass density maps as a weak extrusion from the main cluster at the level of approximately 1% of the peak projected mass

density as shown in the second and fourth rows of Fig. 3. It is interesting to note that these differences that we observe in our simulations are very major, as opposed to relatively minor effects discussed in the literature for such scenarios in the past.

Given the absence of major disruptions in the observed colliding galaxy clusters, the most interesting case currently is that of the weak DM scattering, $a \leq 0.2$ or $\sigma_{DM}/m_{DM} < 0.5\ cm^{-2}g$, shown in the second column of Fig. 3. In that regime, the original DM halos of colliding galaxy clusters are not distorted significantly, yet new features relative to the purely CDM case appear in the post-collision mass distributions. Such differences include heavier and substantially wider central regions of the projected mass density maps, often appearing as bridges connecting the outgoing galaxy clusters at projected mass density levels varying from 1% to 10% of the peak density, as well as somewhat more dispersed DM halos surrounding the outgoing galaxy clusters. The latter effect, that is, the additional dispersion of the DM halos, is seen more prominently in the asymmetric bullet-type collision scenarios in the second and fourth rows of Fig. 3.

A more interesting feature of the projected mass density maps in these scenarios is the remote DM concentrations observed in the equatorial plane of the collisions, absent in CDM simulations. Such features can be seen in the second column of Fig. 3 at the level of 1% of peak density, appearing in the equatorial plane of the collisions at the distances from the collision center similar to that of the outgoing galaxy clusters. The observation of the distant off-axial DM mass densities in weakly scattering regimes can be understood by considering the process of the passage of DM halos through each other during a galaxy cluster collision. In the weak scattering regime, $a \ll 1$, the mean free path of DM particles is substantially greater than the diameter of DM halos. In that case, all DM particles that scatter of each other during the initial passage have a significant chance of leaving their respective DM halos without suffering secondary scattering. This allows a feature to form in a galaxy cluster collision having the form of a DM shell expanding radially away from the center of the collision with the speeds comparable to that of the outgoing galaxy clusters. Such shell provides DM contributions to the projected mass density maps along the equatorial plane of the collision, at close to 90° scattering angles, and at very large distances away from the collision's axis.

Note that the angular distribution of material in such DM ejecta shell in principle should then reflect the microscopic properties of the differential cross-section of DM particle-particle scattering. As a first guess, it is reasonable to suppose that such differential cross-section will be elastic and isotropic. Indeed, the low energy spin-averaged cross-sections of all short-range particle interactions known in physics, including the strong and the weak interactions as well as the scattering cross-section of short-range δ-function-like potentials, are isotropic. Under these assumptions, the DM ejecta shell can be expected to form in a spherically symmetric fashion and expand from the center of the collision with the speed identical to that of the outgoing galaxy clusters. The latter is because the conservation of energy and momentum requires that the relative speeds of DM particles after elastic scattering events are conserved. In the collision's Center-of-Mass reference frame, therefore, such scattered particles will move away from the collision center with exactly the same speed as their non-scattered counterparts, just in different directions. The shell, therefore, will have a narrow radial profile with the width and the shape related to the width and the shape of the colliding DM halos and will move away from the center of the collision in alignment with the outgoing galaxy clusters.

We arrive at the following view of the additional mass component that is introduced into the post-collision mass distributions of colliding galaxy clusters by astrophysically weak DM self-interactions. The additional mass component is a weak spherically symmetric shell expanding radially away from the center of the collision with the speed equal to that of the outgoing galaxy clusters, and moving away radially in-lock with the outgoing galaxy clusters. It links the outgoing galaxy clusters into a single shell-like structure as shown in Fig. 4. At large separations, such DM shell will appear in the projected mass density maps as a dispersed disk-shaped concentration of DM filling the space in between the outgoing galaxy clusters and featuring a thin rim with the width comparable to the size of the original galaxy clusters. It links the colliding galaxy clusters into a ring-like structure, such as shown in the left panel of Fig. 4. In the mass density maps projected along the collision's axis, the same shell will appear as a weak DM ring surrounding the centrally placed galaxy clusters as shown in the right panel of Fig. 4. At early separation stages of the colliding galaxy clusters, such shell will appear as the additional mass contribution in the central region of the collision. Such contribution is provided by the parts of the DM shell scattered directly above and below the collision's center—that is, along the line of observer's sight—and therefore seen as in the right panel of Fig. 4 near the site of the collision for extended periods of time.

IV. OBSERVABILITY CONDITIONS

In this section, we pay attention to the details of the differences introduced by weakly self-interacting DM in the mass distribution of galaxy cluster collisions and discuss in particular the observability of such features as well as the conditions that may favor their astrophysical observation. From the formulation of this problem, it is understood that the observation of weak DM scattering features is challenging, given their extremely low mass density. The

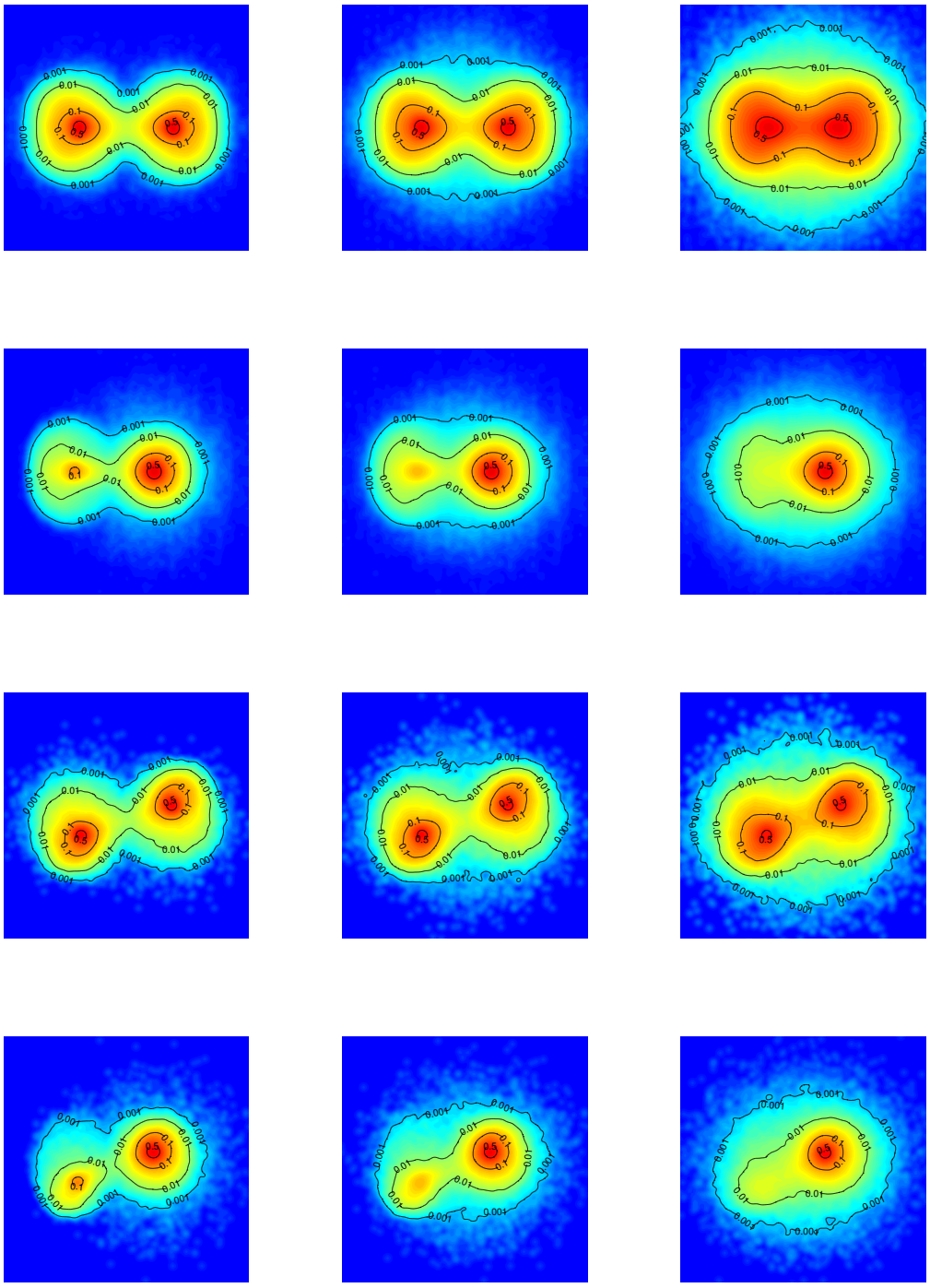

FIG. 3. The phenomenologies of possible post-collision projected mass distributions in collisions of galaxy clusters with self-interacting DM. Different galaxy cluster collision scenarios are shown in different rows: 1st row is central symmetric collisions, 2nd row is central asymmetric collisions, 3rd row is non-central symmetric collisions, and 4th row is non-central asymmetric collisions. Different DM self-interaction strengths are shown in different columns: left column - CDM regime, center column - weak DM scattering regime $a = 0.1$, right column - strong DM scattering regime $a = 0.5$; The kinetic parameter in symmetric collision scenarios is $k = 1.6$ and in asymmetric collision scenarios is $k = 1.4$. The simulation parameters are as defined in Table I.

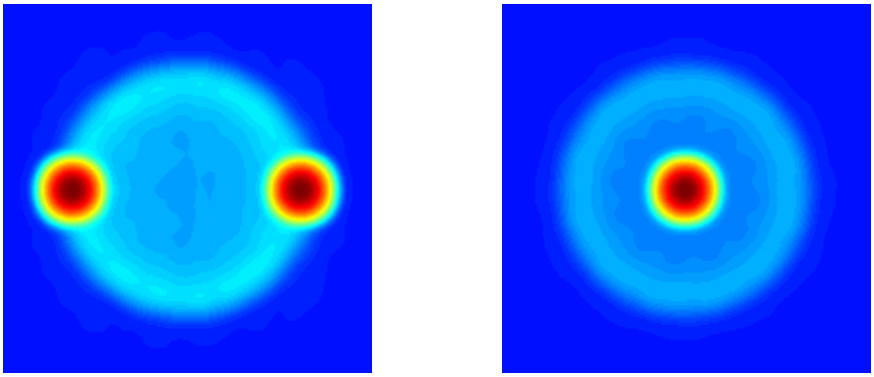

FIG. 4. The mass distribution for a self-interacting DM galaxy cluster collision in an "ideal" scenario where the colliding clusters are very fast and compact. The left panel shows the projected mass density map featuring the radial DM ejecta shell observed along a direction perpendicular to the collision's axis. The right panel shows the same mass density projected along the collision's axis. In the former, the additional DM shell appears as a weak disk-shaped mass distribution with a rim similar in width to the width of the colliding galaxy clusters, extending from the center of the collision radially outwards and linking the outgoing galaxy clusters into a ring-like structure. In the latter, the additional DM shell appears as a weak DM ring surrounding the centrally placed colliding galaxy clusters, seen on top of each other.

DM particle-particle scattering can contribute noticeably 10% to 20% of the entire collision's mass into such shells of scattered DM material without accountable disruptions to the original galaxy clusters, as discussed in the previous section. However, such DM shell weakens as it expands as r^{-2} resulting in the alterations in the projected mass density maps of just about 0.1% to 1% of the peak projected mass density relative to the case of an equivalent CDM mass density model. In this section, we review such alterations carefully. We investigate this question on the example of heavy, symmetric, central galaxy cluster collision, where such differences are expected to be the most pronounced.

A. Comparative analysis of the projected mass distributions of colliding galaxy clusters in the presence of weak DM particle-particle scattering

The differences in the projected mass density maps in weak DM scattering regime are present at all stages of the collisions. Figs. 5-7 present such differences for the values of the kinetic parameter k ranging from 1.5 (moderately fast collision) to 4.0 (very fast collision). In each figure, the projected mass densities for the early separation stage ($\Delta r = 2.5r_c$, where Δr is the distance between the centers of the outgoing galaxy clusters), the intermediate separation stage ($\Delta r = 7.5r_c$) and the late separation stage ($\Delta r = 15r_c$) are shown in immediate comparison with the respective CDM models. The early separation stage corresponds to the colliding galaxy clusters just barely emerging out of the collision, with the separation achieved just at approximately 50% level relative to the peak projected mass density. The intermediate separation stage corresponds to the colliding galaxy clusters that mostly emerged out of the collision, but still have a significant overlap in terms of their r_{200} virial radii and are only separated at about 10% peak-density level. In the late separation stage the colliding galaxy clusters are well separated by a distance close to or exceeding r_{200}.

In the early separation stage, in all scenarios we see quantitative differences in the distribution of mass at the central region of the galaxy cluster collision, whereas the mass distribution in the presence of interacting DM show substantially heavier and wider central densities bridging the outgoing galaxy clusters at high density levels. This difference is seen on the level of 10% to 50% of peak projected mass density and is quite noticeable. The origin of this difference can be traced to the contributions from the parts of the DM ejecta scattered directly above and below the site of collision along the line of sight. Such material can remain near the center of the collision for a longer time and contributes significant excess mass to that region. At small separations, the DM ejecta shell is also more compact and has higher density.

At intermediate separations, the projection of the DM ejecta shell over the collision's center continues to contribute into effectively heavier and wider central regions and more prominent bridges linking the outgoing galaxy clusters,

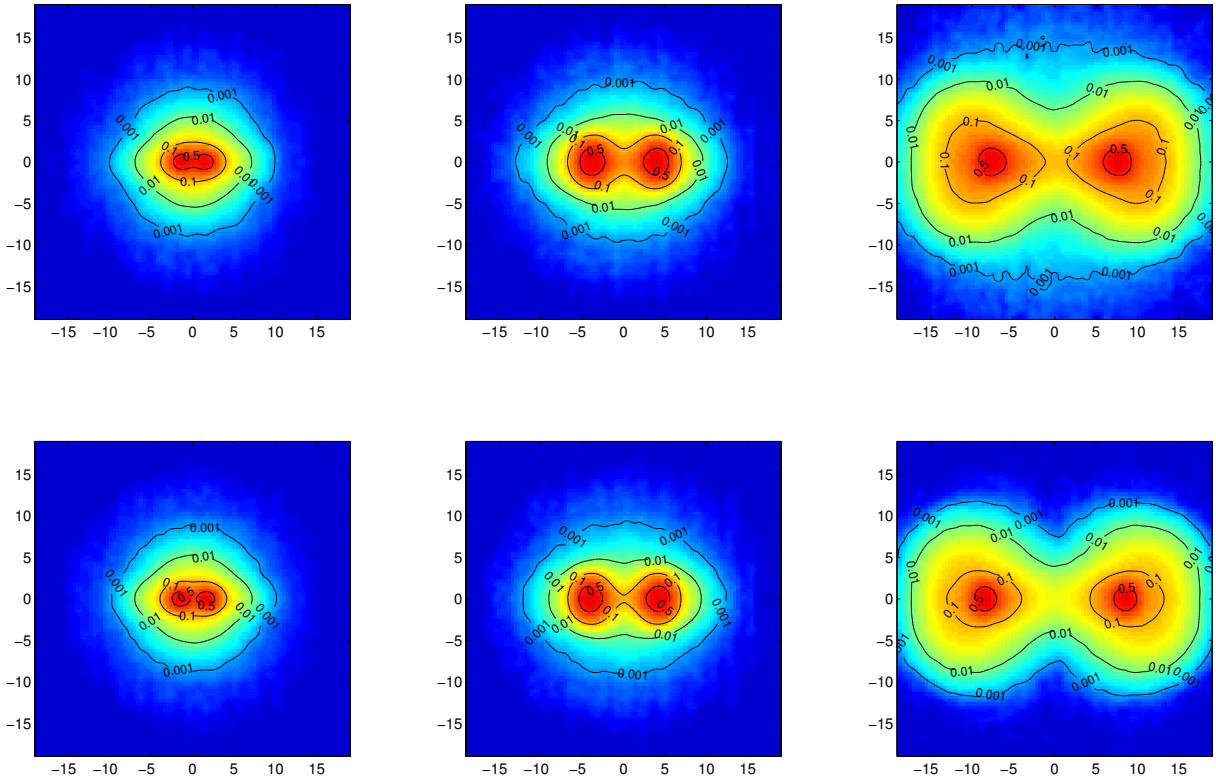

FIG. 5. The difference in the post-collision mass distributions of fast symmetric galaxy cluster collisions with weakly scattering DM and $k = 1.5$. Top row shows the post-collision mass distribution with weakly scattering DM and the bottom row shows the same for standard CDM, for comparison. Three post-collision stages are shown characterized by inter-cluster separation in units of r_c: early stage where the galaxy clusters are just barely separated ($\Delta r = 2.5r_c$, left), intermediate stage where the galaxy clusters just recently became fully separated ($\Delta r = 7.5r_c$, center), and late stage where the galaxy clusters fully separated and moved away to an appreciable distance ($\Delta r = 15r_c$, right). The distance scales are in the units of r_c. The simulation parameters are as in Table I.

even whereas the original galaxy clusters in CDM would be expected to separate at that stage. This effect can be seen at 10% peak-density level. This effect also can be quite noticeable in astrophysical reconstructions of projected mass densities for real colliding galaxy clusters, observed at suitable separation stages.

At late separation stages, the scattered DM ejecta shell begins to emerge as a separate component of the mass density field, introducing not only quantitative but also qualitative differences into the mass distributions of colliding galaxy clusters. Such differences are the most pronounced for galaxy cluster collisions with higher values of the kinetic parameter, $k = 2$ and above, where a distinct oval-shaped shell is seen to form at 0.1% to 1% peak-density levels, as shown in Fig. 6 and Fig. 7. The presence of such shell makes the projected mass density maps in self-interacting DM scenarios look significantly different from the CDM collisions. However, these differences are confined to the tails of the DM halos' mass distributions.

Qualitative differences appear during late separation stages in the mass densities of colliding galaxy clusters projected also along the axis of the collision as shown in Fig. 8. In particular, the scattered DM shell begins to emerge beyond the limits of the original galaxy clusters seen on top of each other in that projection and forms a "bump" or a ring-like feature surrounding these centrally placed outgoing galaxy clusters as seen at 0.1% to 1% peak-density levels.

The shell of scattered DM material continues to be seen in the late stages of lower speed galaxy cluster collisions as well, as shown in the right column of Fig. 5. However, in that case, the shell is superimposed over rather heavy gravitational ejecta and the differences are noticeable only as substantially more disperse shapes of the halos of the outgoing galaxy clusters as seen at 10% peak-density level. Much heavier central density region appears as a bridge connecting the outgoing galaxy clusters at 1% to 10% peak-density levels. The outer rim of the DM ejecta shell emerges

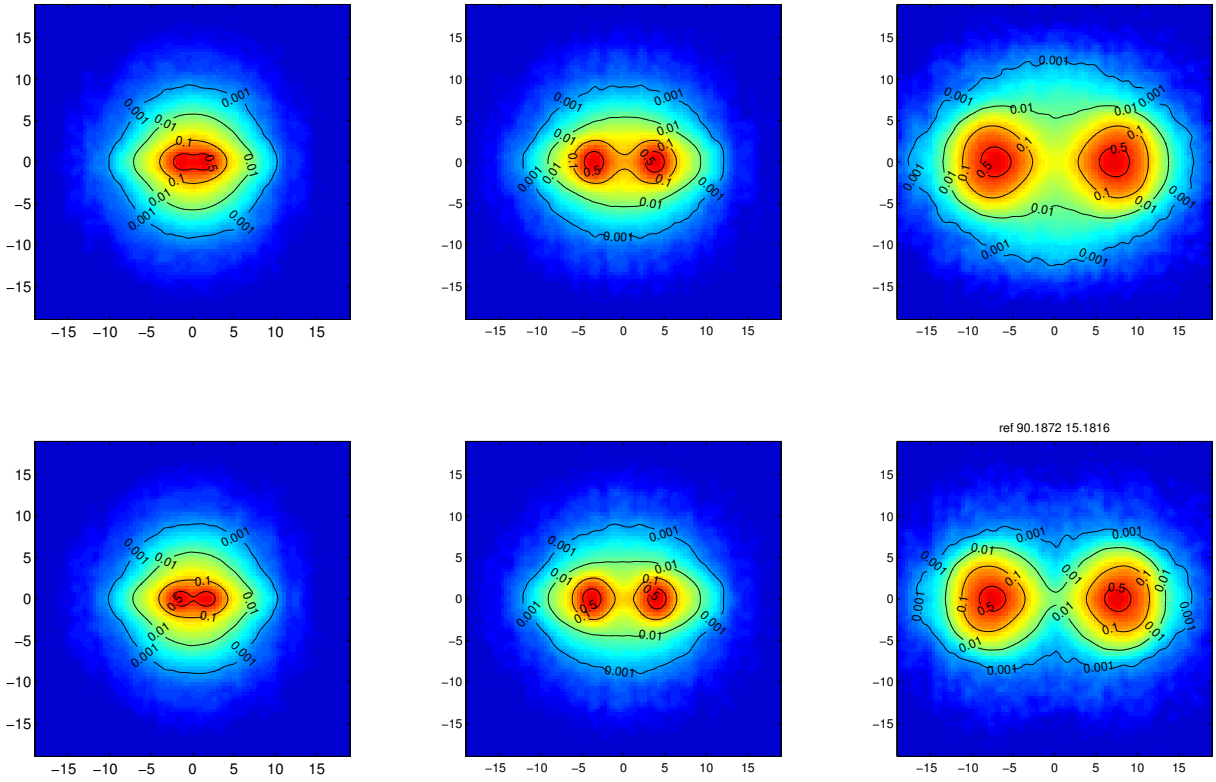

FIG. 6. The difference in the post-collision mass distributions of fast symmetric galaxy cluster collisions with weakly scattering DM and $k = 2.0$. Top row shows the post-collision mass distribution with weakly scattering DM and the bottom row shows the same for standard CDM. Left panels show the mass distributions at early separation stage ($\Delta r = 2.5r_c$), center panels show the mass distributions at intermediate separation stage ($\Delta r = 7.5r_c$), and right panels show the mass distributions at late separation stage ($\Delta r = 15r_c$). The distance scales are in the units of r_c. The simulation parameters are as in Table I.

at 0.1% to 1% density levels only in the equatorial plane at distances of $(5 - 10)r_c$. In the projections observed along the collision's axis, the DM ring cannot be seen clearly under these conditions due to the heavy forward gravitational ejecta reaching the distances as large as $10r_c$.

B. Quantitative measures of the weak DM scattering effects in projected mass distributions

The qualitative differences observed in the previous section for the central regions of colliding galaxy clusters in the presence of self-interacting DM can be captured quantitatively by plotting the projected mass density along the line connecting the centers of the outgoing galaxy clusters. Such mass profiles for self-interacting DM and CDM are shown in Fig. 9.

At the early separation stages, the difference in the projected mass density in the central regions of the galaxy cluster collisions in interacting DM and CDM scenarios is clearly seen from these plots. Such differences reach 10% of peak-density and are very substantial. In the case of slower galaxy cluster collisions, left panel in Fig. 9, the significant differences in the central mass densities continue to persist throughout all post-collision stages, in agreement with the qualitative observations made in the previous section. In the later stages of the collisions, the central region in that scenario features as much as two times more mass than in a comparable CDM collision. Slower collision scenarios also feature a lag of DM halos in the interacting DM scenarios relative to CDM counterparts. This lag is the reflection of lower outgoing velocities of the colliding galaxy clusters in the presence of interacting DM, and thus can be most clearly seen in the late stages of the collision as $0.7 - 0.8r_c$ offset in the positions of interacting DM halos relative to CDM. The same lag can be seen in these simulations in the intermediate stage as the lag of about $0.3 - 0.4r_c$.

The differences in such "axial" mass density plots, both in terms of the density differences and the lag, decrease

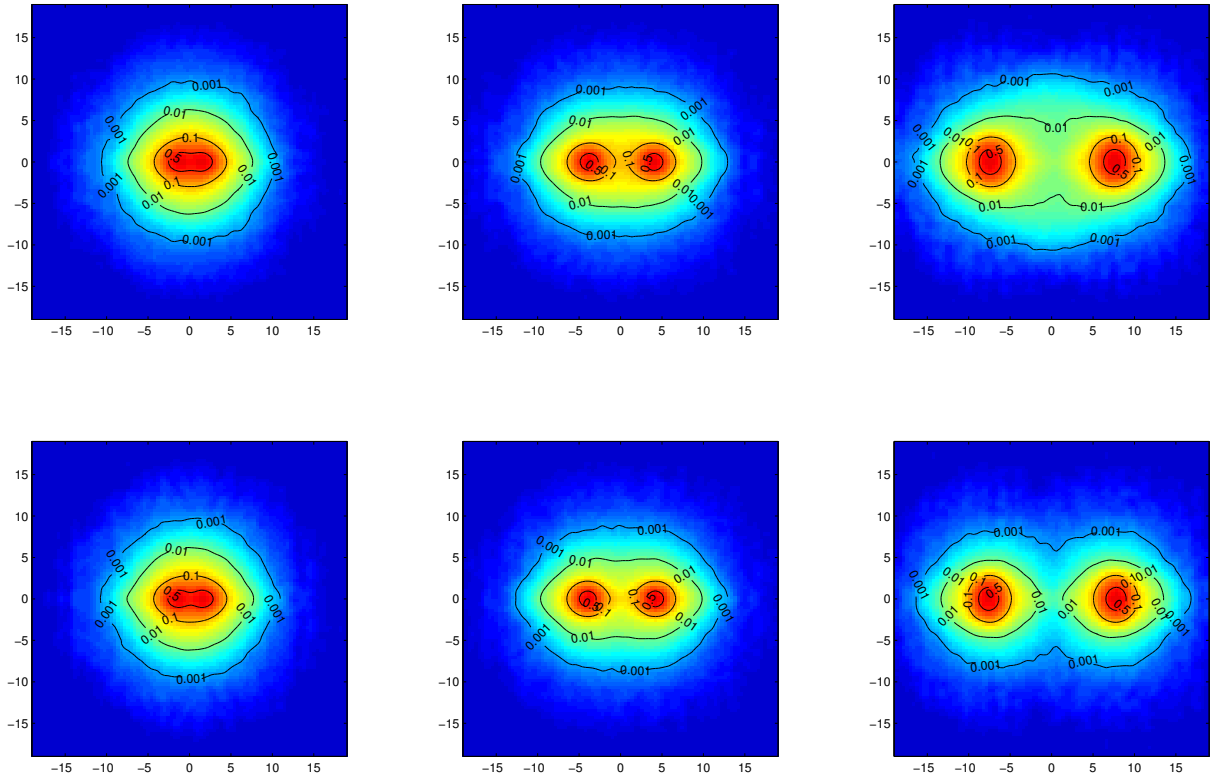

FIG. 7. The difference in the post-collision mass distributions of fast symmetric galaxy cluster collisions with weakly scattering DM and $k = 4.0$. Top row shows the post-collision mass distribution with weakly scattering DM and the bottom row shows the same for standard CDM. Left panels show the mass distributions at early separation stage ($\Delta r = 2.5r_c$), center panels show the mass distributions at intermediate separation stage ($\Delta r = 7.5r_c$), and right panels show the mass distributions at late separation stage ($\Delta r = 15r_c$). The distance scales are in the units of r_c. The simulation parameters are as in Table I.

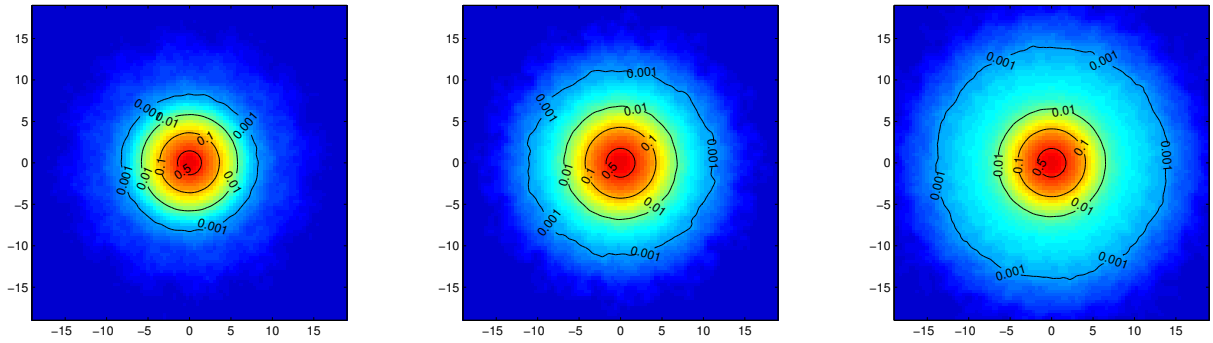

FIG. 8. The shell of scattered DM material surrounding the colliding galaxy clusters in the post-collision mass distribution seen along the axis of the collision. Left panel shows the post-collision mass distribution for very fast colliding galaxy clusters in standard CDM, seen in that projection. Center and right panels show the same post-collision mass distributions for weakly scattering DM, as seen at late ($\Delta r = 15r_c$) and very late ($\Delta r = 25r_c$) separation stages, respectively. $k = 4.0$ in these simulations. The distance scales are in the units of r_c. The simulation parameters are as in Table I.

with the increase of the kinetic parameter k. In particular, while one continues to see a noticeable 10-15% difference

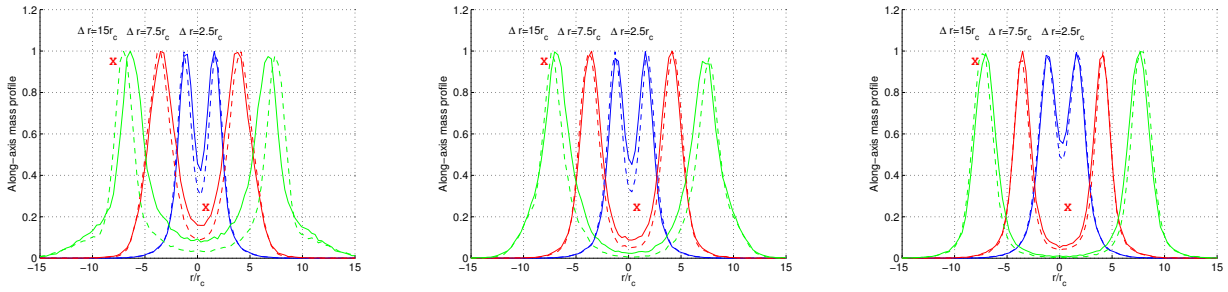

FIG. 9. The projected mass density plotted along the line connecting the centers of the colliding galaxy clusters for the collisions with different values of the kinetic parameter k and different post-collision separation stages. Shown are such mass density plots for early ($\Delta r = 2.5r_c$), intermediate ($\Delta r = 7.5r_c$) and late ($\Delta r = 15r_c$) post-collision separation stages, for weakly interacting DM (solid lines) and CDM (dashed lines), for $k = 1.5$ (left), $k = 2.0$ (center) and $k = 4.0$ (right). The differences between interacting DM and CDM models focused upon in the main text are shown with the symbol "X".

in the central mass densities in the early separation stages in the middle ($k = 2.0$) and right ($k = 4.0$) panels of Fig. 9, such differences all but disappear in the late separation stages. There is also no consistently seen lag in the outgoing DM halos in these cases. Such lag becomes negligible as the speed of the colliding galaxy clusters increases with k.

One of the differences in the projected mass density maps of the colliding galaxy clusters in the presence of interacting DM is the spherical shell of scattered DM material which contributes mass at remote locations and the directions perpendicular to the collision axis. Such spherical shell formation is impossible in purely gravitational high-speed collisions. The plot which quantifies the galaxy cluster collision's mass contained in the sectors at the center of the collision with various scattering angles can provide a quantitative measure of that effect. In particular, one expects to see a uniform DM density or density excess in the presence of a shell of isotropically scattered DM material, whereas one expects such a plot for CDM galaxy cluster collisions to drop close to zero once the scattering angle approaches 90°.

Fig. 10 provides the plots for the projected mass density contained in 15° degree sectors at the center of the collision as the function of the angle counted from the collision's equatorial plane. In the case of CDM, one expects such plots to decrease to zero at angles close to 0° (that is, near the equatorial plane). In the presence of the shell of self-scattered DM material, one expects to see a flat segment extending from large negative to large positive angles around 0°. Indeed, this is the behavior that we see in Fig. 10. The difference between CDM and interacting DM cases can be seen for all collision speeds and separation stages, but most prominently for high k and late separation stages. In particular, there is no mass density contributed to sectors around the collision's equator in CDM, while there is still as much as 1% of mass contributed per sector in interacting DM scenarios.

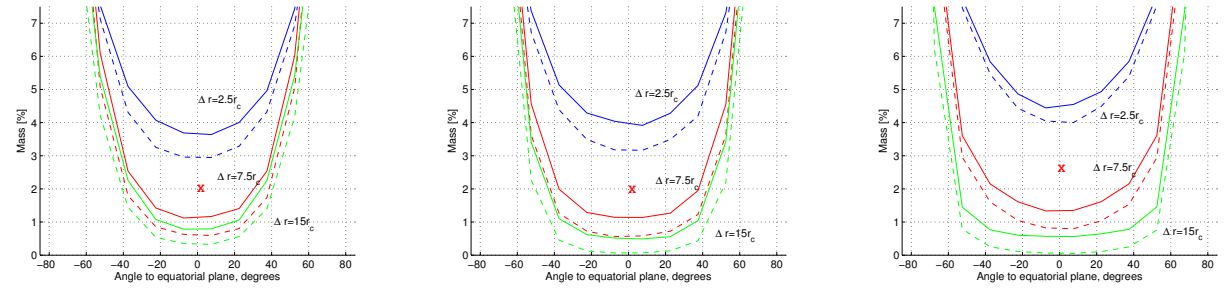

FIG. 10. The plots of the mass contained in projected mass density maps in 15° degree sectors centered on the collision's center, as a function of the angle to the collision's equatorial plane, and shown as the percentile of the total density map's mass. Shown are the respective plots for early ($\Delta r = 2.5r_c$), intermediate ($\Delta r = 7.5r_c$) and late ($\Delta r = 15r_c$) post-collision separation stages, for weakly interacting DM (solid lines) and CDM (dashed lines), for $k = 1.5$ (left), $k = 2.0$ (center) and $k = 4.0$ (right). The differences between interacting DM and CDM models focused upon in the main text are shown with the symbol "X".

Another feature of the scattered DM shell is the presence of DM at large scattering angles as well as large distances

from the collision's center. In fact, this feature can be seen at about the same distances as that of the outgoing galaxy clusters. As illustrated in Fig. 11, this feature can be quantitatively inspected by plotting the distribution of mass in the projected mass density maps inside a narrow 15° to 30° sector around the equatorial plane as a function of the distance from the collision's center.

Fig. 12 shows such plots in the units of percentile of the total projected mass per $1r_c$ distance interval inside the sector $[-30°, 30°]$, for intermediate and late separation stages of different galaxy cluster collisions. Clear difference between interacting DM and CDM can be seen in Fig. 12, either for intermediate or late separation stages. In the late stages of very fast galaxy cluster collisions, the difference is particularly profound. In CDM, we see practically no contribution in the right panel of Fig.12 (dashed line for $\Delta r = 15r_c$) as expected, while in interacting DM scenarios we see consistent concentrations of DM at the correct distances (that is, approximately the distance of the galaxy clusters to the collision center). In the case of the galaxy cluster collisions with $k = 1.5$, the left panel in Fig. 12 still shows a clear difference between interacting DM and CDM cases. Although there are significant mass contributions in the equatorial sector also in CDM case for $k = 1.5$, these contributions occur only at the distances $r/r_c < 5$ and do not extend to very large radii such as $r/r_c > 5 - 7$. Note that the separation Δr in Fig. 12 is that between the centers of the colliding galaxy clusters, so that the distance from the clusters to the collision center is $\Delta r/2$.

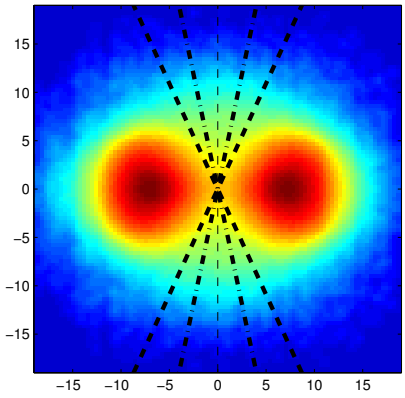

FIG. 11. The presence of the shell of scattered DM material can be quantitatively detected by plotting the projected mass distribution in a narrow equatorial sector as the function of the distance from the collision's center. Shown in this illustration is such quantification, using two sectors covering $[-15°, 15°]$ (bold dash-dotted line) and $[-30°, 30°]$ (bold dotted line) angles around the equatorial plane (thin dashed line).

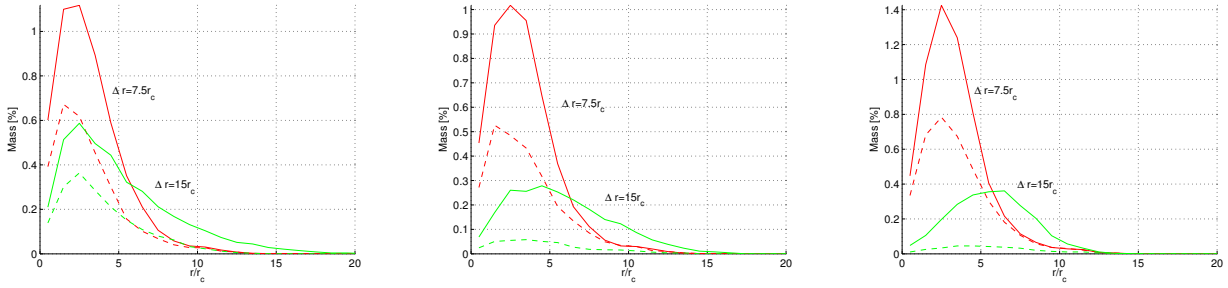

FIG. 12. The plot of the distribution of mass in the projected density maps inside a $[-30°, 30°]$ sector around the collision's equatorial plane, as a function of the distance from the collision center. Shown are respective plots for intermediate ($\Delta r = 7.5r_c$) and late ($\Delta r = 15r_c$) post-collision separations, for weakly interacting DM (solid lines) and CDM (dashed lines), for $k = 1.5$ (left), $k = 2.0$ (center) and $k = 4.0$ (right).

Finally, we consider the observability of the scattered DM shell in the mass density maps projected along the collision's axis appearing as a ring surrounding the centrally located colliding galaxy clusters, such as illustrated in

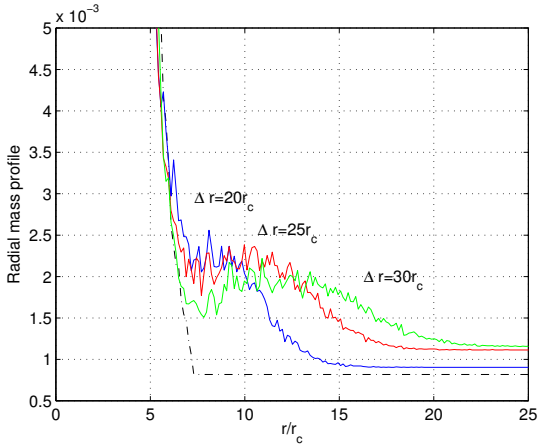

FIG. 13. The scattered DM shell in the tail of the radial mass profile of a very high speed galaxy cluster collision observed along the collision's axis at very late separation stages.

the right panel of Fig. 4. We find that such feature can be observed only in the very fast galaxy cluster collisions at very late separation stages, whereas the scattered DM shell essentially needs to move beyond the galaxy clusters' virial radii and appear on top of the surrounding background. Despite the weak magnitude of that effect, the observation of such shells might be the most dramatic confirmation of the self-interacting nature of DM. An example of such a shell in the tails of the radial mass profile of colliding galaxy clusters seen along the collision axis is shown in Fig. 13. In Fig. 13, the size of the feature associated with the scattered DM shell is just about 0.2% of the peak-density. However, the size of that feature can be larger for the collisions of more compact galaxy clusters, and can be estimated using the following approximate formula,

$$\frac{\rho_{shell}}{\rho_{max}} = 2\beta a \frac{\log(1+c)}{r/r_c}, \tag{7}$$

where $\beta \approx 0.5$ is a numerical factor characterizing the magnitude of the terminal rise in the projection of the edge of the spherical shell relative to its central densities, a is the fraction of the DM halo scattered into the DM shell, c is the galaxy clusters' concentration parameter, and r is the current radius of the shell. Given Eq.(7), we can estimate the mass excess observed in such radial mass profiles to be between 0.1% and 3%. Note that Ref. [27] reports such a "narrow" ring-like feature with the excess of approximately 1% to 5% in the long-range reconstructions of the radial mass profile of the galaxy cluster CL 0024+17.

C. The difference from NFW-like mass profiles

The equilibrium mass profile that was used in this work differs in several important ways from the NFW mass profile, commonly used to describe the mass distribution in virialized galaxy clusters. In this section, we address the differences that are introduced in our results due to such differences from the NFW profile as well as from the King model's profile, $\rho(r) = \rho_o/(1 + r^2/r_c^2)^{3/2}$, thereby referred to as the King profile. The King profile had been used in the literature as an alternative for the NFW mass profile for soft-core SIDM halos [21, 28].

First, our equilibrium profile has a soft core in contrast to the NFW mass profile as shown in Fig.1. Soft cores are generally expected for SIDM halos based on general arguments as well as the results of numerical simulations [49]. While early studies suggested that SIDM soft cores could be ruled out by catastrophic core collapse observed in simulations [5, 52], recent full cosmological studies with high-resolution have shown that a broad range of SIDM particle mass and cross-sections could produce soft-core DM halos that are stable on the scales of Hubble time [53, 54]. Additionally, some recent theoretical works suggested that singular cusps in NFW profiles may be in fact numerical artifacts of N-body dynamics rather than a real physical effect [55–57]. The observational evidence for soft versus cuspy cores in galaxy clusters is likewise inconclusive. While some recent studies indicate a good agreement with cusped NFW profiles for many known galaxy clusters, there are equally large number of results in the literature implicating soft cores in many galaxy clusters (see [50, 51] as well as [12, 58] for a recent review).

With respect to the effect of DM self-interactions on the collisions of galaxy clusters, the differences introduced by a central cusp will be narrowly localized to the halos' centers and therefore will have little impact on the effects considered in this work. The alterations introduced by the central cusp are confined to somewhat different DM particle-particle scattering rates—higher at the collision's center due to the larger density of the NFW central cusp but also briefer in time due to such cusps' much smaller dimensions. Somewhat narrower cross-section profile of the scattered DM shell also occurs. The narrower cross-section profile has little consequence for the appearance of such shells in the projected mass density maps, as long as the total mass of the shell remains unchanged. The narrow cross-section translates in a slightly more noticeable rim around the projected image of the shell, as shown in Fig. 14.

The differences in the scattering rate for cuspy and soft-core mass profiles can be estimated theoretically, using

$$a \ = 2\frac{\sigma_{DM}}{m_{DM}} \int d^2 r \Sigma_1(\vec{r}+\vec{b})\Sigma_2(\vec{r})/M_{tot}, \tag{8}$$

where a is the fraction of DM halo mass scattered via DM particle-particle collisions, $\Sigma_{1,2}(\vec{r})$ are the projected mass densities of the two colliding galaxy clusters, and $\vec{b}$ is the vector denoting the impact parameter. For NFW-like mass profiles, Eq. (8) depends on the value of the concentration parameter c of the colliding galaxy clusters. For a central collision of two equal massive NFW DM halos with $c = 4$, we obtain using Eq. (8) that the NFW profile produces just about 10% more DM particle scatterings than the Plummer profile and about 55% more DM particle scatterings than the King profile. Given the typical range of the concentration parameters known for galaxy clusters, $c = 4-8$, we can also find that for $c = 8$ the NFW profile produces approximately 50% fewer DM particle scattering than the Plummer profile and close to 40% more DM particle scatterings than the King profile. Furthermore, the net scattering rate is significantly higher for the galaxy clusters with lower concentration parameter c. The galaxy clusters with $c = 4$ scatter approximately 2 times as much DM halo's mass as that with $c = 8$.

In the simulations, these differences in the scattering rate can be elementarily removed by adjusting the value of the numerical DM interaction parameter α. Thus, it only affects the physical interpretation of the simulations' results by means of Eq. (2) in Section II.

Overall, we conclude that the differences introduced to our results by the DM halos' profiles potentially having a cuspy center instead of a core are insignificant.

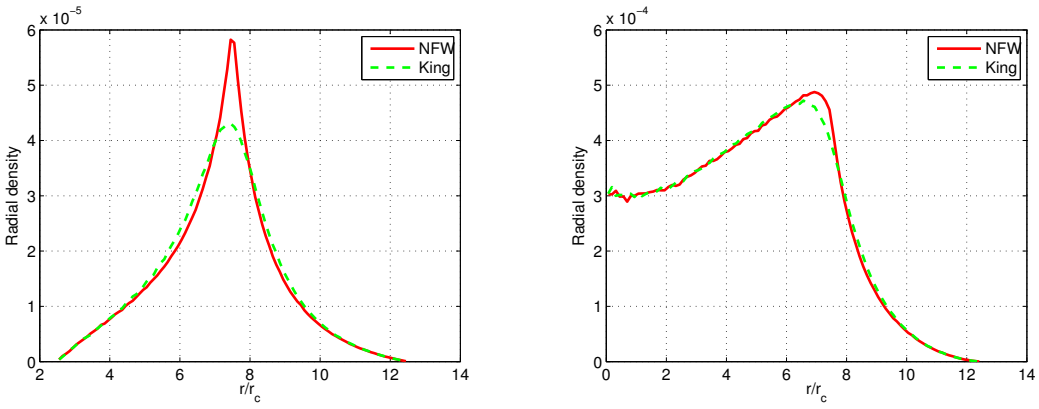

FIG. 14. A comparison of 3D (left panel) and projected mass density (right panel) radial profiles of the scattered DM shell for a cuspy (NFW) and a soft-core (King) mass profile.

The second difference of our equilibrium mass profile from the mass profiles such as the NFW or the King profile is the significantly faster decay at larger distances than either the NFW or the King profile. Whereas the NFW and the King profiles decay at large distances as r^{-3}, the Plummer profile used here has asymptotic r^{-5} behavior. It can be noted, however, that the Plummer profile does look close to the King profile at all distances out to about r_{200} as shown in Fig. 15. Thus, one can expect the post-collision mass distributions such as modeled by the Plummer profile to be reasonably similar to that obtained by using the NFW, or more properly—the King profile out to the post-collision separations of up to $\Delta r \approx 8-10r_c$. These expectations are born out by direct simulations as shown in Figs. 16-20.

With respect to the late and very late separation stages, such as $\Delta r = 15r_c$ and above, an additional complication needs to be considered. At those stages, the scattered DM shell has actually moved outside the virial radius of the colliding galaxy clusters. To properly evaluate how this situation may be different with NFW-like mass profiles, it is necessary to account how the NFW profile behaves at the distances greater than the virial radius.

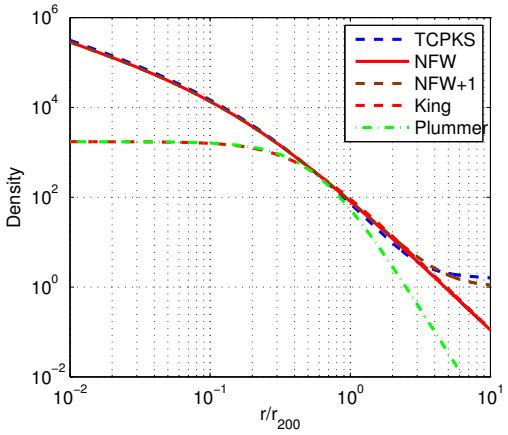

FIG. 15. The long-range behavior of the DM halo mass profiles in CDM, according to [59]. The radial mass profile from [59] is shown for a massive galaxy cluster with $c = 5$ as TCPKS curve, out to the estimated range of validity of $10r_{200}$. The y-axis is in the units of the critical density ρ_{crit} and the x-axis is in the units of the virial radius r_{200}. One can see that beyond the virial radius the DM mass profiles can be assumed to fall as r^{-3} out to the distances $4 - 5r_{200}$, after which the density becomes essentially a constant on the order of ρ_{crit}. Other mass profiles such as the King profile and the Plummer profile are also shown. One can see, in particular, that the Plummer profile is a reasonably good approximation for the mass distribution in heavy galaxy clusters (aside from the central cusp/core) almost entirely out to their virial radii r_{200}.

While such "beyond-r_{200}" density behavior received little attention in the literature, recent N-body simulations [59, 60] indicate that the NFW mass profile should continue to fall after r_{200} with essentially the same law r^{-3} out to approximately the critical density ρ_{crit} at the distances $3 - 5r_{200}$. At that point, the density becomes a constant on the order of ρ_{crit} as shown in Fig. 15. This behavior is of course different from the Plummer profile, which falls off much more sharply beyond r_{200}[61].

In the case of the NFW and the King profile, therefore, the shell of scattered DM material is observed on top of r^{-3} background till very late separation stages. This results in the projected mass distributions that look numerically different from those inspected in previous sections. However, simulations show that the same DM self-scattering effects continue to be seen under these conditions as well. Figs. 16-20 show the results of such simulations using the NFW and the King DM mass profiles for very fast galaxy cluster collisions.

D. Optimal observation conditions

In the previous sections we have seen that the differences in the post-collision mass distributions of colliding galaxy clusters related to self-interacting nature of DM can be observed in different forms during different stages of a galaxy cluster collision. It is found that the most profound such differences are located in the space between colliding galaxy clusters but not inside them. These differences can be understood in terms of spherical shells of singly-scattered DM particles engulfing the outgoing original galaxy clusters. These shells may contain up to 10% to 20% of the combined colliding galaxy clusters' mass without the original galaxy clusters themselves suffering profound distortions.

At the early and intermediate post-collision separation stages, the parts of such shells scattered directly above and below the collision center—that is along the line of observer's sight—can contribute to the creation of significantly heavier and wider centers in the projected mass density maps of galaxy cluster collisions as shown in Figs. 5-7 as well as in Figs. 16-18. The differences in that region are very substantial during early post-collision separation stages, contributing to the increase in the central densities relative to CDM collisions for up to 10%-20%. Up to the 2-fold increase can be seen during late separation stages for the collisions with lower values of the kinetic parameter k as shown in Fig. 9 as well as in Fig. 19. Lag in the centers of DM halos for self-interacting DM can be observed for fast ($k \approx 1.5$) but not very fast ($k > 2$) collisions from Fig. 9. These differences can be quantitatively described by using the plots of projected mass density along the line connecting the centers of the outgoing galaxy clusters as shown in Fig. 9 and Fig. 19.

The magnitudes of these features are no doubt rather large and amenable to the measurement. At the same time, convincingly discerning such features from real observations may face significant challenges. For instance, the above central mass excess overlays and is of similar magnitude with the slow baryonic component of the colliding galaxy

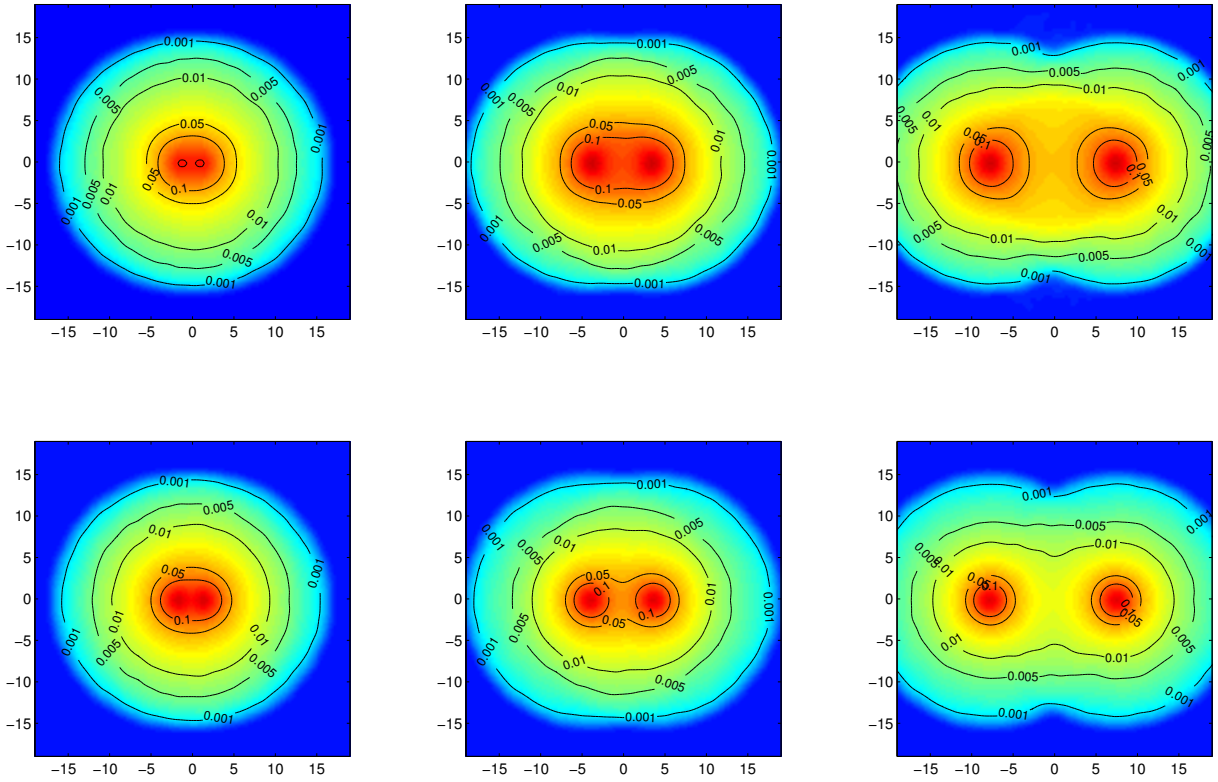

FIG. 16. The post-collision mass distribution of a fast symmetric galaxy cluster collision ($k = 4.0$) with the DM halos modeled using the NFW mass profile. Top row shows the post-collision mass distribution for weakly scattering DM and the bottom row shows the post-collision mass distribution for CDM. Post-collision separation stages are shown for early ($\Delta r = 2.5r_c$, left), intermediate ($\Delta r = 7.5r_c$, center) and late ($\Delta r = 15r_c$, right) stages. The distance scales are in the units of the scale radius of the NFW profile.

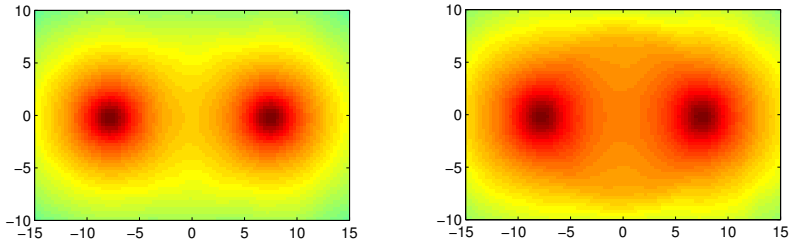

FIG. 17. The central part of the projected mass density maps from the right panel of Fig. 16, shown without the level contours to emphasize the centrally-placed shell of scattered DM material in the post-collision mass distribution. The left panel is CDM and the right panel is interacting DM. The shell of scattered DM particles appears clearly in this log-scale projected mass density map at the level of 1% to 5% of peak-density. See the right panel of Fig. 16 for the version of this figure with the level contours.

clusters. Therefore, such baryonic contributions may need to be accurately subtracted from the central regions of colliding galaxy clusters in order to demonstrate the presence of DM self-scattering excess reliably. Establishing the excess of DM in the central regions of galaxy cluster collisions by means of numerical simulations may suffer from the sensitivity to initial conditions such as the initial velocity of the colliding galaxy clusters, their mass, their concentration parameters, and even any unknown substructure. With the view of these difficulties, the observation of galaxy cluster collisions at intermediate post-collision separations may offer greater advantages since the modifications

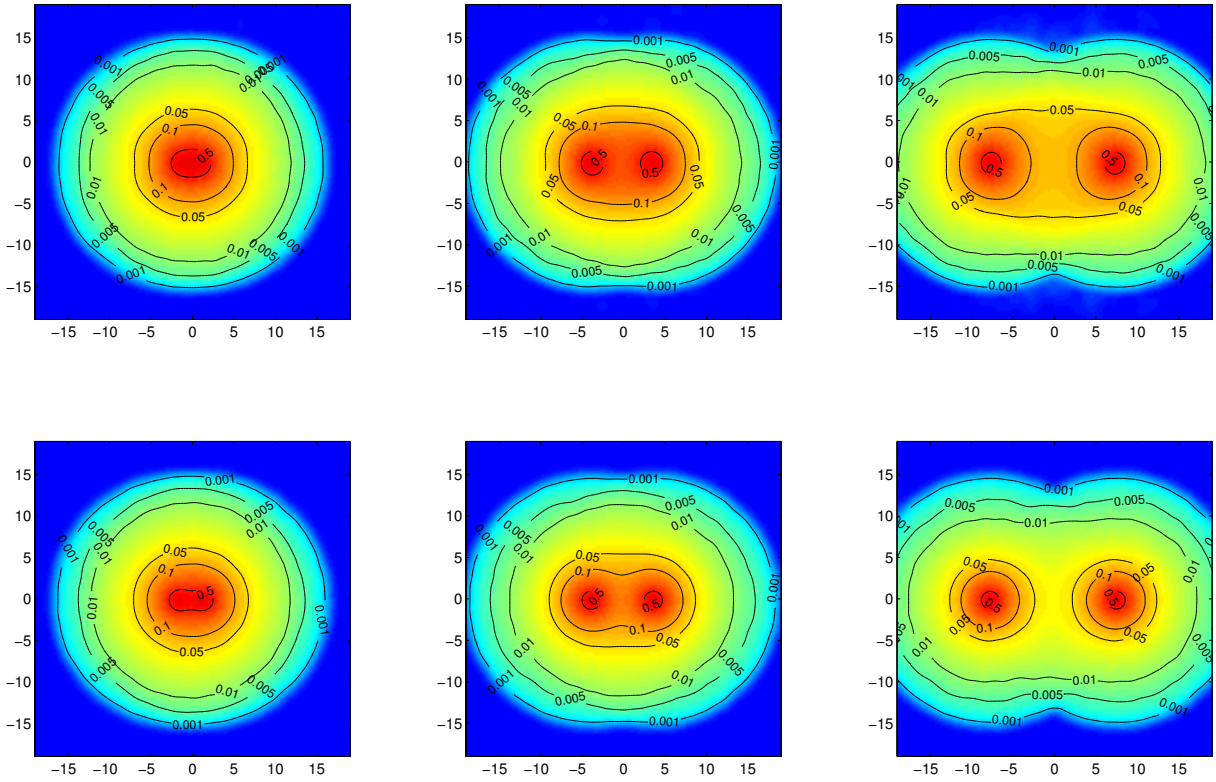

FIG. 18. The post-collision mass distribution of a fast symmetric galaxy cluster collision ($k = 4.0$) with the DM halos modeled using the King mass profile. Top row shows the post-collision mass distribution for weakly scattering DM and the bottom row shows the post-collision mass distribution fpr CDM. Post-collision separation stages are shown for early ($\Delta r = 2.5r_c$, left), intermediate ($\Delta r = 7.5r_c$, center) and late ($\Delta r = 15r_c$, right) stages. The distance scales are in the units of the King profile's scale parameter (same as the core radius r_c).

seen in the central regions of such collisions due to the self-interacting nature of DM occupy a significantly greater spatial extent.

The lag of self-interacting DM halos behind their noninteracting analogs has been another popular target of analysis in the literature. We see in Fig. 9 that such lag indeed may reach impressive magnitudes during late post-collision separations. At the same time, the experimental measurement of such a lag faces a separate set of challenges. Ideally, one would want to have an example of the same galaxy cluster collision in the absence of DM self-interactions, in order to establish such a lag. That is of course impossible. The centroids of the galaxy groups associated with the colliding galaxy clusters had been used instead as the proxy for such collisionless examples. However, the galaxy groups do not represent such an ideal example. In particular, such galaxy groups move in the gravitational field of their respective DM halos and are slowed by them, should the DM halo begin to fall behind. The lag estimated by using such galaxy groups' centroids, therefore, is subject to underestimation bias that needs to be quantified. Estimating the lag from simulations of galaxy cluster collisions can be affected by the problems of unknown initial conditions, as mentioned above. In particular, as we see in Fig. 9, the magnitude of the lag drops rapidly with collision's speed. Already for $k = 2$, we do not see any appreciable lag in the positions of colliding self-interacting DM or CDM halos. Finally, the ability to define the centroids of the galaxy groups and the DM distributions with required precision has been called into question recently.

A qualitative new feature is observed in the the projected mass density maps of galaxy cluster collisions in the presence of self-interacting DM during late post-collision separation stages. Such feature is a large expanding shell of scattered DM material surrounding the outgoing galaxy clusters. Such shell produces mass contributions to the projected mass density maps at 0.1%-5% peak-density levels at very large distances from the collision center and large scattering angles. This feature can be quantified by using azimuthal plots of the mass distribution in the projected mass density maps around the collision's center, or by using the plots of mass density inside small (30°) sectors around

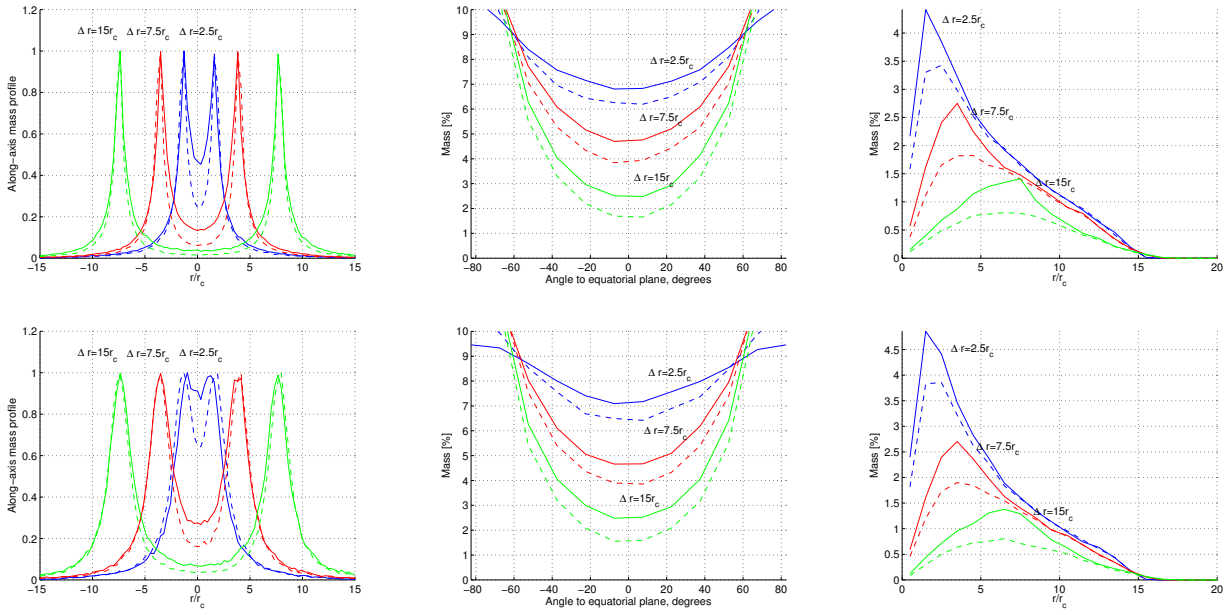

FIG. 19. The DM self-interaction related measures discussed in the previous section, shown for the collision of NFW and King DM halos, the top row and the bottom row, respectively. The residual mass densities seen in the azimuthal and equatorial sectoral mass plots (middle and right column) for CDM case are the contributions made by the post-virial radius mass densities, surrounding the colliding galaxy clusters. Clearly such background contributions would normally be subtracted, leading to the azimuthal and equatorial sectoral mass plots for interacting DM case much similar to that obtained in our simulations (which naturally did not include such beyond-r_{200} mass densities), Fig. 10 and 12.

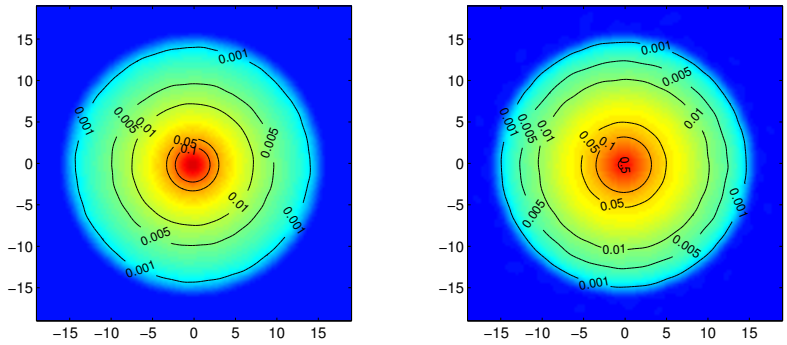

FIG. 20. In the mass density projected along the collision's axis, scattered DM shell appears in the medium and late separation stages as a significant widening of the region of 1%-5% density, with respect to the other parts of the radial density profile. If scattered DM shell moves further outwards and into the region of constant ρ_{crit} background density, then a ring-like shell structure can also appear in that projection, as had been discussed in previous sections. The simulation is for the NFW mass profile. Left panel shows CDM case and right panel is interacting DM case.

the collision's equatorial plane at the collision's center (see Figs. 10, 12 and 19). In all such cases, significant deviations from CDM case can be observed in the presence of self-interacting DM. For very late separation stages, when the scattered DM shell moves into the region of constant background density surrounding the colliding galaxy clusters (that is, well beyond their virial radii), a ring-like DM shell structure can become also visible in the mass densities projected either perpendicular to or along the collision's axis. The distinctiveness of these features is enhanced by greater collision speed and greater compactness of the colliding galaxy clusters.

Given these, we can suggest that the observation of collisions of galaxy clusters with high speed and small concen-

tration parameters at intermediate and late post-collision separations will provide the most favorable conditions for observing the effects of DM self-interactions using the projected mass density maps of such collisions. With respect to the collisions' speed, the higher k above 2.0 is certainly preferred because it leads to much lesser gravitational disruptions of the original colliding galaxy clusters and eases the process of subtracting the background mass densities for clearer identification of the DM self-interaction contributions. High speed of galaxy clusters does not affect the DM particle-particle scattering, as such speed cancels out from the DM self-scattering effects. That is, the higher collision speed results in exactly the same amount of self-scattered DM material as a lower one. On the other hand, the efficiency of gravitational effects decreases with higher speed.

Higher values of the kinetic parameter for a galaxy cluster collision means that the colliding galaxy clusters need to in-fall from finite speeds at infinity. Tables II and III list the initial in-fall and the closest-approach speeds corresponding to different values of k for different collision masses M_{tot}. As can be seen from these tables, for very heavy galaxy clusters the initial speed required to achieve $k \approx 2-4$ is high but not prohibitively so. The closest-approach speeds may appear high, but one should remember that a substantial part of these is the speed gained from the gravitational acceleration of the clusters themselves during the in-fall. The initial in-fall speeds required to achieve a given k drop with the total mass of the collision. For instance, the required initial in-fall speed is 1000 kmps for $k = 2$ and $M = 10^{14} M_{\odot}$. Such initial speeds are quite feasible in the context of galaxy clusters' relative motion within a superstructure such as a galaxy supercluster. They are also achievable if the galaxy clusters collided after in-falling towards a filament of the large-scale structure. Examples of galaxy cluster collisions hypothesized to have occurred near a filament are indeed known [38].

TABLE II. The initial clusters' in-fall speeds in relation to the collision's kinetic parameter k and the collision's total mass M_{tot}.

k	$10^{15} M_{\odot}$	$5 \cdot 10^{14} M_{\odot}$	$10^{14} M_{\odot}$	$5 \cdot 10^{13} M_{\odot}$	$10^{13} M_{\odot}$
1	0 kmps	0 kmps	0 kmps	0 kmps	0 kmps
2	2100 kmps	1700 kmps	1000 kmps	800 kmps	470 kmps
4	3600 kmps	2900 kmps	1700 kmps	1400 kmps	780 kmps
8	5600 kmps	4400 kmps	2500 kmps	2100 kmps	1200 kmps

TABLE III. The closest approach relative collision speeds in relation to the the collision's kinetic parameter k and the collision's total mass M_{tot}.

k	$10^{15} M_{\odot}$	$5 \cdot 10^{14} M_{\odot}$	$10^{14} M_{\odot}$	$5 \cdot 10^{13} M_{\odot}$	$10^{13} M_{\odot}$
1	4200 kmps	3300 kmps	1900 kmps	1500 kmps	900 kmps
2	5900 kmps	4700 kmps	2800 kmps	2200 kmps	1300 kmps
4	8400 kmps	6600 kmps	3900 kmps	3100 kmps	1800 kmps
8	11900 kmps	9300 kmps	5500 kmps	4400 kmps	2600 kmps

V. SUMMARY AND DISCUSSION

In this work, we performed simulations to study possible phenomenologies of the post-collision mass distributions in high-speed galaxy cluster collisions such as the Bullet cluster 1E 0657-56, MACSJ 0025-1222, Abel520, Abel754, etc. With respect to the self-interactions of DM, the possible phenomenologies of such galaxy cluster collisions can be characterized essentially by two parameters — the ratio of the kinetic and gravitational energy in the collision, k, and the fraction of the mass of DM halos scattered during the collision via DM particle-particle interactions, a.

With respect to the kinetic parameter k, we find three main regimes in our simulations. For the collisions with very high speed $k > 2$, the galaxy clusters tend to pass through each other largely undisturbed. For the collisions with smaller but still high speed $2 > k > 1$, the collisions typically produce axial "fan-out" ejecta of the material from DM halos via gravitational effects. This gravitational ejecta, though, is observed to be confined to small scattering angles in the forward and backward cones around the axis of the collision. For yet slower collisions, we distinguish "free-fall" ($k = 1$) and slow ($k < 1$) collisions. In both of these cases, the kinetic energy of the colliding clusters is insufficient to ensure their complete separation after the first passage, and a rapid merger ensues producing widespread and disperse gravitational ejecta in the post-collision mass distributions.

With respect to the self-scattering of DM particles, we find three main types of the post-collision mass distribution. For strong DM self-scattering, in which 50% or more of the DM halo particles scatter during the initial passage of the colliding galaxy clusters through each other, $a > 0.5$ or $\sigma_{DM}/m_{DM} > 2cm^{-2}g$, we observe that the DM halos are rapidly destroyed in the collision. This disruption is severe and results in the formation of a common single halo composed of highly heated DM material. As such, this outcome is far beyond the limited effects restricted to the changes in mass-to-light ratio or a lag of DM halos, which were previously discussed in the literature. Instead, complete and rapid reorganization of the entire DM halos of the colliding galaxy clusters is seen. We don't observe the formation of dark central cores discussed in certain papers in the literature. This can be explained by a large amount of energy released into DM halos during such collisions.

For weak DM self-scattering, in which 10% to 20% of DM halo particles suffer a non-gravitational scattering, $a \approx 0.1 - 0.2$ or $\sigma_{DM}/m_{DM} < 0.5cm^{-2}g$, the formation of spherical shells of singly-scattered DM particles is observed. This can be understood by considering the scattering of DM particles on each other during the initial passage of colliding galaxy clusters through one another, under the conditions that the mean free path of DM particles is significantly greater than the size of the halos, which is certainly the case for $a \ll 1$. The shell of scattered DM material can be observed from the projected mass density maps of colliding galaxy clusters. It can be obtained with gravitational lensing reconstructions as a disk-shaped diffuse DM density centered at the collision's center having a thin ring-like rim of varying degree of clarity to a large extent. This shell always extends out and engulfs the original galaxy clusters. In that, it must have a unique and well-defined size. Such shells can contribute significant DM material to the locations of projected mass density maps at large distances from the collision's center and large scattering angles close to 90°. This feature is forbidden for strictly gravitational ejecta. The large extent of such DM feature makes it also distinct from the baryonic component of colliding galaxy clusters such as the hot intra-cluster gas.

Previous analyses of the properties of DM particles for observed collisions of galaxy clusters typically focused on the examination of the absence of any major disruptive effects in the DM halos of the colliding galaxy clusters [17, 21, 22, 28, 31, 35, 43]. These effects included the change in the mass-to-light ratio and the drag or the lag of the DM halos relative to their corresponding galaxy groups. In the present study, we focus on possible galaxy cluster collision scenarios in the presence of astrophysically weak DM self-interactions to show that these may impart subtle yet noticeable features in the distribution of mass in galaxy cluster collisions outside of the colliding galaxy clusters. We find that the DM material scattered during galaxy cluster collisions via such DM particle-particle scattering can appear in projected mass density maps as DM structures at very large scattering angles and large distances from the collision's center. Such structures are forbidden in purely gravitational collision scenarios, whereas the ejecta formed by purely gravitational effects is concentrated in high speed collisions only in the forward and the backward cones around the collision's axis. The weak DM self-scattering structures appear as a spherical shell of DM material engulfing the outgoing galaxy clusters in strict alignment with them, and may admit up to 20% of the total collision's mass before disruptions to the main DM halos become apparent. Depending on the post-collision separation stage of colliding galaxy clusters, such shells may produce distinctive contributions to the projected mass density maps ranging from 0.1% to 10% of the peak mass density.

The remote location of such scattered DM mass densities either from the outgoing galaxy clusters or the central hot ICM gives hope that such structures can be observed under favorable conditions. The survey of the literature on the weak and strong gravitational lensing reconstructions of the mass profiles of colliding galaxy clusters shows that the presence of DM densities at large scattering angles and large-distance is, in fact, quite typical in such reconstructions. The projected mass densities in the colliding galaxy clusters A754 and A520 both show significant off-axial DM concentrations at close to 90° scattering angle and roughly the correct distance from the collision's center [29, 38]. Combined weak and strong lensing reconstructions of the projected mass density in the Bullet cluster in [23] also show wide, diffuse, disk-like mass concentration in between the outgoing galaxy clusters and having roughly the correct size. Even more interesting is the recent observation of a ring-like DM structure in the long-range reconstructions of the mass profile of strongly lensing galaxy cluster CL0024+017, now figured as a galaxy cluster collision seen along the collision axis. Such reconstruction indicated a weak ring-like DM structure surrounding the colliding galaxy clusters as shown in Fig. 7 and Fig. 10 of Ref. [27]. This structure may be the remains of a scattered DM shell discussed in this work, although the magnitude of this structure found in Ref. [27] may be a bit large with respect to our simulations.

Our results provided a generic view on the phenomenology of the post-collision mass distributions in the collision of galaxy clusters in the presence of self-interacting DM. They may help guide future numerical simulation studies of real colliding galaxy clusters. Focusing on the potential DM self-scattering features that we identified, it may be useful to examine the astrophysical reconstruction of the mass distributions in colliding galaxy clusters from weak and strong gravitation lensing.

Appendix A: Dark Matter Particle Scattering Algorithm and Particle Mesh Algorithm

Algorithm 1 DM particle-particle scattering algorithm

for all $cell \in \mathcal{G}$ **do**
  for all particles $i, j \in cell$ **do**
    Select the pair (i, j) with probability $P = \alpha|\vec{v}_i - \vec{v}_j|\Delta t$
    if selected **then**
      $\vec{V}_{CM} \leftarrow (\vec{v}_i + \vec{v}_j)/2$
      $V_{rel} \leftarrow |\vec{v}_i - \vec{v}_j|/2$
      Choose $\vec{n}$ uniformly at random on unit sphere
      $\vec{v}_i \leftarrow \vec{V}_{CM} + V_{rel}\vec{n}$
      $\vec{v}_j \leftarrow \vec{V}_{CM} - V_{rel}\vec{n}$
    end if
  end for
end for

Algorithm 2 Particle Mesh algorithm for N-body gravitational dynamics

Require: simulation parameters $M_{tot}, N1, N2, \Delta V2, \Delta R1, \Delta R2, \Delta b$
Require: $\mathcal{G}$ is a cubic 3D grid of size D^3
Require: $list \leftarrow \{(\vec{r}_i, \vec{v}_i)\}$ is the list of particles' position and velocity vectors
  {Form initial particle distributions for the two colliding clusters}
  $list1 \leftarrow N1$ random particles from the standard equilibrium profile (Section II A)
  $list2 \leftarrow N2$ random particles from the standard equilibrium profile (Section II A)
  $scaling1 \leftarrow ((M_{tot}N1/(N1+N2))/M_{std})^{1/3}$
  $scaling2 \leftarrow ((M_{tot}N2/(N1+N2))/M_{std})^{1/3}$
  Update all particles in $list1 : \vec{r}_i \leftarrow \vec{r}_i \cdot scaling1, \vec{v}_i \leftarrow \vec{v}_i \cdot scaling1$
  Update all particles in $list2 : \vec{r}_i \leftarrow \vec{r}_i \cdot scaling2, \vec{v}_i \leftarrow \vec{v}_i \cdot scaling2$
  Update all particles in $list1 : (\vec{r}_i)_x \leftarrow (\vec{r}_i)_x - \Delta R1$, $(\vec{r}_i)_y \leftarrow (\vec{r}_i)_y - \Delta b$
  Update all particles in $list2 : (\vec{r}_i)_x \leftarrow (\vec{r}_i)_x + \Delta R2$

  {Calculate initial in-fall velocities}
  $\Delta R \leftarrow \Delta R1 + \Delta R2$
  $E_G \leftarrow \frac{G(M_{tot})^2}{\Delta R}(\frac{N1}{N1+N2})(\frac{N2}{N1+N2})$
  $V2 \leftarrow \frac{2E_G}{M_{tot}} + \Delta V2$
  Update all particles in $list1 : (\vec{v}_i)_x \leftarrow (\vec{v}_i)_x + \sqrt{\frac{N2}{N1}V2}$
  Update all particles in $list2 : (\vec{v}_i)_x \leftarrow (\vec{v}_i)_x - \sqrt{\frac{N1}{N2}V2}$

  $list \leftarrow \{list1, list2\}$

  {Main simulation loop}
  while $t < t_{max}$ **do**
    $\Delta t \leftarrow \min(\Delta t_{max}, \Delta r_{max}/\max(|\vec{v}_i|))$
    Discard the particles that moved out of the bounds of $\mathcal{G}$
    Distribute the particles in $list = \{\vec{r}_i, \vec{v}_i\}$ into the cells of grid $\mathcal{G}$ based on $\vec{r}_i \in cell$, $n(\vec{x}) \leftarrow list\{\vec{r}_i\}$
    $\tilde{n}(\vec{k}) \leftarrow FFT(n(\vec{x}))$
    $\tilde{\Phi}(\vec{k}) \leftarrow -4\pi\tilde{n}(\vec{k})/k^2$ (but set $\tilde{\Phi}(0) \leftarrow 0$)
    $\Phi(\vec{x}) \leftarrow iFFT(\tilde{\Phi}(\vec{k}))$
    For all particles in $list : \vec{a}_i \leftarrow -G\nabla\Phi(\vec{r}_i)$
    $\Delta t \leftarrow \min(\Delta t, \Delta v_{max}/\max(|\vec{a}_i|))$
    Update all particles in $list : \vec{v}_i \leftarrow \vec{v}_i + \vec{a}_i\Delta t$
    Evaluate particle-particle scatterings using Algorithm 1
    Update all particles in $list : \vec{r}_i \leftarrow \vec{r}_i + \vec{v}_i\Delta t$
    $t \leftarrow t + \Delta t$
  end while

ACKNOWLEDGMENTS

This work was supported in part by the American Physical Society International Travel Grant Award Program (APS ITGAP) and in part by the US Department of Energy under Contract NO. DE-FG02-03ER41260. This research also used the resources of the National Energy Research Scientific Computing Center (NERSC), which is supported by the Office of Science of the U.S. Department of Energy under Contract No. DE-AC02-05CH11231. YM also would like to acknowledge the support from the Bilim Akademisi—The Science Academy (Istanbul, Turkey) young investigator award under the BAGEP program.

[1] G. Bertone, D. Hooper, and S. J, Physics Reports, **405**, 279 (2005).
[2] L. Baudis, Nuclear Physics B, **235-236**, 405 (2013).
[3] M. R. Buckley and P. J. Fox, Physical Review D, **81**, 083522 (2010).
[4] R. Cyburt, B. Fields, V. Pavlidou, and B. Wandelt, Physical Review D, **65**, 123503 (2002), arXiv:0203240 [arXiv:astro-ph].
[5] C. S. Kochanek and M. White, Astrophysical Journal, **534**, 514 (2000).
[6] A. Pontzen and F. Governato, Nature, **506**, 171 (2014), ISSN 1476-4687.
[7] B. D. Wandelt, R. Dave, C. R. Farrar, P. C. McGuire, D. N. Spergel, and P. J. Steinhardt, arXiv:astro-ph/0006344 (2000).
[8] N. Yoshida, V. Springel, and S. D. M. White, Astrophysical Journal, **535**, L103 (2000).
[9] R. Massey, L. Williams, R. Smit, M. Swinbank, T. Kitching, and D. Harvey, Monthly Notices of the Royal Astronomical Society, **449**, 3393 (2015).
[10] Y. Mishchenko and C.-R. Ji, Physical Review D, **68**, 063503 (2003), ISSN 0556-2821.
[11] L. L. R. Williams and P. Saha, Monthly Notices of the Royal Astronomical Society, **415**, 448 (2011).
[12] D. H. Weinberg, J. S. Bullock, F. Governato, R. K. de Naray, and A. H. G. Peter, Proceedings of the National Academy of Sciences of the United States of America, **112**, 12249 (2015).
[13] R. Foot, Physics Letters B, **728**, 45 (2014), ISSN 03702693.
[14] M. V. Medvedev, Physical Review Letters, **113**, 071303 (2014).
[15] Y. Hochberg, E. Kuflik, T. Volansky, and J. G. Wacker, Physical Review Letters, **113**, 171301 (2014).
[16] D. M. Jacobs, G. D. Starkman, and B. W. Lynn, arXiv:1410.2236 (2014).
[17] M. Bradac, Nuclear Physics B - Proceedings Supplements, **194**, 17 (2009), ISSN 09205632.
[18] M. Bradac, S. W. Allen, T. Treu, H. Ebeling, R. Massey, R. G. Morris, A. von der Linden, and D. Applegate, Astrophysical Journal, **687**, 959 (2008).
[19] D. Clowe, M. Bradac, A. H. Gonzalez, M. Markevitch, S. W. Randall, C. Jones, and D. Zaritsky, Astrophysical Journal Letters, **648**, L109 (2006), arXiv:0608407v1 [arXiv:astro-ph].
[20] D. Clowe, S. Randall, and M. Markevitch, Nuclear Physics B - Proceedings Supplements, **173**, 28 (2007), ISSN 09205632.
[21] D. Clowe, A. Gonzalez, and M. Markevitch, Astrophysical Journal, **604**, 596 (2004), arXiv:0312273v1 [arXiv:astro-ph].
[22] M. Markevitch, A. H. Gonzalez, D. Clowe, A. Vikhlinin, W. Forman, C. Jones, S. Murray, and W. Tucker, Astrophysical Journal, **606**, 819 (2004), arXiv:0309303v2 [arXiv:astro-ph].
[23] M. Bradac, D. Clowe, A. H. Gonzalez, P. Marshall, W. Forman, C. Jones, M. Markevitch, S. Randall, T. Schrabback, and D. Zaritsky, Astrophysical Journal, **652**, 937 (2006).
[24] G. W. Angus, B. Famaey, and H. S. Zhao, Monthly Notices of the Royal Astronomical Society, **371**, 138 (2006).
[25] V. Springel and G. R. Farrar, Monthly Notices of the Royal Astronomical Society, **380**, 911 (2007).
[26] A. Mahdavi, H. Hoekstra, A. Babul, D. D. Balam, and P. L. Capak, Astrophysical Journal, **668**, 806 (2007), ISSN 0004-637X.
[27] M. J. Jee, H. C. Ford, G. D. Illingworth, R. L. White, T. J. Broadhurst, D. A. Coe, G. R. Meurer, A. van der Wel, N. Benitez, J. P. Blakeslee, R. J. Bouwens, L. D. Bradley, R. Demarco, N. L. Homeier, A. R. Martel, and S. Mei, Astrophysical Journal, **661**, 728 (2007).
[28] S. W. Randall, M. Markevitch, D. Clowe, A. H. Gonzalez, and M. Bradac, Astrophysical Journal, **679**, 1173 (2008).
[29] N. Okabe and K. Umetsu, arXiv:astro-ph/0702649, 1 (2008), arXiv:0702649v4 [arXiv:astro-ph].
[30] A. Nusser, Monthly Notices of the Royal Astronomical Society, **384**, 343 (2008).
[31] C. Mastropietro and A. Burkert, Monthly Notices of the Royal Astronomical Society, **389**, 967 (2008).
[32] S. Deb, D. M. Goldberg, and V. J. Ramdass, Astrophysical Journal, **687**, 39 (2008), ISSN 0004-637X.
[33] D. Coe, N. Ben, T. Broadhurst, and L. A. Moustakas, Astrophysical Journal, **722**, 1 (2010).
[34] K. Umetsu, T. Broadhurst, A. Zitrin, E. Medezinski, and L.-y. Hsu, Astrophysical Journal, **729**, 127 (2011).
[35] J. Merten, D. Coe, R. Dupke, R. Massey, A. Zitrin, E. S. Cypriano, N. Okabe, B. Frye, F. G. Braglia, Y. Jimenez-Teja, N. Benitez, T. Broadhurst, J. Rhodes, M. Meneghetti, L. A. Moustakas, L. Sodre Jr., J. Krick, and J. N. Bregman, Monthly Notices of the Royal Astronomical Society, **417**, 333 (2011), arXiv:arXiv:1103.2772v3.
[36] B. Ragozzine, D. Clowe, M. Markevitch, a. H. Gonzalez, and M. Bradač, Astrophysical Journal, **744**, 94 (2012), ISSN 0004-637X.
[37] J. Kneib, J. Richard, A. Morandi, M. Limousin, and E. Jullo, arXiv:1209.0384 (2012), arXiv:arXiv:1209.0384v1.

[38] M. J. Jee, A. Mahdavi, H. Hoekstra, A. Babul, J. J. Dalcanton, P. Carroll, and P. Capak, Astrophysical Journal, **747**, 96 (2012), ISSN 0004-637X.

[39] D. Clowe, M. Markevitch, M. Bradač, A. H. Gonzalez, S. M. Chung, R. Massey, and D. Zaritsky, Astrophysical Journal, **758**, 128 (2012), ISSN 0004-637X.

[40] C. Lage and G. Farrar, arXiv: astro-ph/1312.0959 (2013), arXiv:arXiv:1312.0959v1.

[41] A. Paredes and H. Michinel, arXiv: 1512.05121 (2015).

[42] F. S. Guzman, J. A. Gonalez, and J. P. Cruz, arXiv: 1605.04856 (2016).

[43] D. Harvey, R. Massey, T. Kitching, A. Taylor, and E. Tittley, arXiv:1503.0767 (2015).

[44] D. Sijacki and V. Springel, Monthly Notices of the Royal Astronomical Society, **366**, 397 (2006), arXiv:0509506 [arXiv:astro-ph].

[45] G. W. Angus and S. S. Mcgaugh, Monthly Notices of the Royal Astronomical Society, **383**, 417 (2008).

[46] H. Dejonghe, Monthly Notices of the Royal Astronomical Society, **224**, 13 (1987).

[47] G. Bertin, "Dynamics of galaxies," (Cambridge University Press, 2000) Chap. 22.2, pp. 319–330.

[48] J. F. Navarro, C. S. Frenk, and S. D. White, Astrophysical Journal, **462**, 563 (1996).

[49] R. Dave, D. N. Spergel, P. J. Steinhardt, and B. D. Wandelt, Astrophysical Journal, **547**, 574 (2001).

[50] A. B. Newman, T. Treu, R. S. Ellis, D. J. Sand, C. Nipoti, J. Richard, and E. Jullo, Astrophysical Journal, **765**, 24 (2013).

[51] A. B. Newman, T. Treu, R. S. Ellis, and D. J. Sand, Astrophysical Journal, **765**, 25 (2013).

[52] A. Burkert, Astrophysical Journal, **534**, L143 (2000).

[53] M. Rocha, A. H. Peter, J. S. Bullock, M. Kaplinghat, S. Garrison-Kimmel, J. Onorbe, and L. A. Moustakas, Monthly Notices of the Royal Astronomical Society, **430**, 81 (2013).

[54] A. H. G. Peter, M. Rocha, J. S. Bullock, and M. Kaplinghat, Monthly Notices of the Royal Astronomical Society, **430**, 105 (2013).

[55] A. N. Baushev, Astrophysical Journal, **786**, 65 (2014).

[56] A. N. Baushev, Astroparticle Physics, **62**, 47 (2015).

[57] A. N. Baushev, L. del Valle, L. E. Campusano, A. Escala, R. R. Munoz, and G. A. Palma, arXiv:1606.02835 (2016).

[58] A. Del Popolo and M. Le Delliou, "Small scale problems of the Λcdm model: a short review," (2016).

[59] H. Tavio, A. J. Cuesta, F. Prada, A. A. Klypin, and M. A. Sanchez-Conde, arXiv:0807.3027 (2008).

[60] F. Prada, A. A. Klypin, E. Simonneau, J. Betancort-Rijo, S. Patiri, S. Gottlober, and M. A. Sanchez-Conde, Astrophysical Journal, **645**, 1001 (2006).

[61] Note that should one have simulated NFW or King DM halos' collision by truncating at r_{200}, one would obtain for heavy galaxy clusters nearly the identical result to that presented in the previous sections, based on the use of the Plummer density profile, given that the Plummer profile matches the NFW profile (or rather the King profile) well in the region of distances smaller than r_{200}.